J Nanopart Res (2021) 23: 204
https://doi.org/10.1007/s11051-021-05254-w

REVIEW

Application of supercritical fluid in the synthesis of graphene materials: a review

Yoong Xin Pang · Maxine Yew · Yuxin Yan · Pan Khine · Andrew Filbert · Sivakumar Manickam · Dominic C. Y. Foo · Nusrat Sharmin · Edward Lester · Tao Wu · Cheng Heng Pang

Received: 18 November 2020 / Accepted: 1 June 2021 / Published online: 31 August 2021

Abstract The studies on the utilisation of supercritical fluids (SCFs) in processing chemicals and materials have garnered significant attention in the past two decades. SCFs possess both gas- and liquid-like properties that are tunable, rendering them as superior solvents for reactions and processes, for example in the delamination of graphite. SCF technologies are deemed to be potential alternatives to existing technologies for graphene production that are yet to be industrially scalable. This review features recent works on the production of graphene facilitated by SCFs, with emphasis on the conversion of graphite to graphene through exfoliation and reduction. The exfoliation processes report the yield of 6 to 27% of monolayer graphene and 3 to 25% of ≤ 5 layers of graphene, whilst the carbon-to-oxygen (C/O) ratio of graphene produced via different reduction processes ranges from 0.37 to 28.2 with interlayer spacing of 0.35 to 0.38 nm. Recent applications of gas-expanded solvents for the synthesis of graphene and

Y. X. Pang · C. H. Pang (✉)
Department of Chemical and Environmental Engineering, University of Nottingham Ningbo China, Ningbo 315100, People's Republic of China
e-mail: chengheng.pang@nottingham.edu.cn

M. Yew
Department of Mechanical, Materials and Manufacturing, University of Nottingham Ningbo China, Ningbo 315100, People's Republic of China

Y. Yan · C. H. Pang
Municipal Key Laboratory of Clean Energy Conversion Technologies, University of Nottingham Ningbo China, Ningbo 315100, China

P. Khine · A. Filbert · T. Wu
New Materials Institute, University of Nottingham Ningbo China, Ningbo 315100, People's Republic of China

S. Manickam
Petroleum and Chemical Engineering, Faculty of Engineering, Universiti Teknologi Brunei, Bandar Seri Begawan BE1410, Brunei Darussalam

D. C. Y. Foo
Department of Chemical and Environmental Engineering/ Centre of Excellence for Green Technologies, University of Nottingham Malaysia, 43500 Semenyih, Selangor, Malaysia

N. Sharmin
Department of Process Technology, Nofima AS, 4021 Stavanger, Norway

E. Lester
Department of Chemical and Environmental Engineering, University of Nottingham, Nottingham NG7 2RD, UK

T. Wu
Key Laboratory for Carbonaceous Wastes Processing and Process Intensification Research of Zhejiang Province, University of Nottingham Ningbo China, Ningbo 315100, People's Republic of China

the fabrication of functionalised graphene materials via SCF-aided processes are also described. In addition, a summary of the properties of common SCFs as well as the characterisation of graphene materials, such as the number of layers, C/O ratio, interlayer spacing, pore size and surface area, is included to provide insights on the process efficiency.

Keywords Supercritical fluid · Nanomaterials · Exfoliation · Reduction · Characterisation

Introduction

Research on the production of graphene and its applications is trending as graphene demonstrates remarkable thermal, electrical and mechanical properties (Allen et al. 2010). Numerous applications based on graphene materials have been and are still being developed across different fields of science and technology. Graphene possesses superlative electrical conductivity and has been found to have profound use in energy storage for batteries and supercapacitors (Pruna et al. 2013) as well as in other potential applications that include drug delivery, disease diagnostic tools (Salem 2020) and development of sensors (Yi 2013). Such interests and demands for graphene have led to intense investigations on the synthesis of high-quality graphene in large scale. Existing methods for the synthesis of graphene are categorised as top-down and bottom-up approaches. The very first manner from which graphene was derived was through careful peeling off layers from graphite with scotch tapes. For obvious reasons, this approach is not scalable, thus leading to graphene derivation through bottom-up graphene growth from precursors, through top-down mechanical abrasions or through solvent-driven synthesis. Various solvents have been applied, and supercritical fluids are notably one of the solvents receiving significant attention.

A fluid is supercritical when its temperature and pressure are above the critical points (Eckert et al. 1996). At supercritical state, fluids possess both gas- and liquid-like physicochemical properties such as near-zero surface tension, low viscosity, high solvating power and diffusion coefficients (Sun et al. 2019). The intriguing properties of supercritical fluids (SCFs) have been explored and applied to materials processing, in particular, on the design, development and production of particles, for example 2D materials (Bahrami and Ranjbarian 2007). Bahrami and Ranjbarian reviewed the production of microcomposite and nanocomposite particles by $ScCO_2$ and distinguished the synthesis of composite materials according to the role of $ScCO_2$ as solvent, anti-solvent, solute and reaction medium. Likewise, substantial works are being directed towards the synthesis of graphene via SCFs following the advent of SCF technologies (Bahrami and Ranjbarian 2007). Thus far, Gao and Hu (Gao and Hu 2016) have produced a rather comprehensive review on this topic whilst Sun et al. (2019) considered SCF-facilitated exfoliation and processing of 2D materials including graphene materials in recent years. In this paper, the utilisation of SCFs for the synthesis of graphene is critically reviewed, with emphasis on the intercalation and exfoliation of stacked graphene layers into isolated sheets. More recent works on the reduction of graphene oxide have also been included.

Conventional methods for the synthesis of graphene

Carbon, one of the common elements on earth, forms various allotropes (Kharisov and Kharissova 2019) including graphite, diamond, amorphous carbon and glassy carbon. A new form of carbon of only one atom thick known as graphene was discovered in 2004. It is a 2D material and is commonly produced from graphite with sp^2-bonded carbon atoms arranged in a honeycomb structure (Geim and Novoselov 2010). Chemically stable and transparent graphene is known to be stronger than diamond. It demonstrates a mechanical strength of 130 GPa (Zhu 2010), Young's modulus of about 1 TPa (Lee 2013) and a large specific surface area of 2630 $m^2\ g^{-1}$ (Zhu 2010). Also, it has an excellent electrical conductivity with charge mobility of 200,000 $cm^2\ V^{-1}\ s^{-1}$ (Bolotin 2008; Lozowski 2010) and thermal conductivity of approximately 5000 $W\ m^{-1}\ K^{-1}$ (Balandin 2008) owing to delocalised electrons over the plane. The phenomenal chemical and physical properties of graphene have attracted interest in nanotechnology research, and a substantial number of studies have been carried out to establish production methods to obtain high-quality graphene. Carbon-rich materials such as graphite (Berger 2004) are commonly preferred as the starting materials for the synthesis of graphene. Recent studies have also explored the replacement of natural graphite with biochar, a solid product derived from biomass processing

(Yan 2016) via pyrolysis (Lester 2018; Pang et al. 2018) or gasification processes (Parvez 2016), which contains graphite microcrystalline structure (Fang 2020), and have demonstrated successful production of graphene. Biomass such as urea (Pan 2013), petals (Ray 2012) and food waste (Ruan 2011) are used as starting materials for graphene synthesis. However, the production of biochar might emit pollutants such as mercury (Zhao 2016, 2015), nitrogen and sulphur oxides (Zhao 2020) if the selected biomass categories are not carefully considered before processing. Therefore, further research on biomass properties is needed to achieve efficient production without compromising on environmental sustainability. In general, graphene synthesis techniques are categorised into bottom-up and top-down approaches as illustrated in Fig. 1.

Bottom-up approaches

Bottom-up approaches such as chemical vapour deposition (CVD), epitaxial growth and flame synthesis entail the growth of graphene from atomic-sized precursors. CVD process takes place at elevated temperatures of 650–1000 °C (Min 2014) to grow graphene sheets on metallic catalysts (Lee 2019; Dayou 2017). Hydrocarbon gases decompose into free carbon and hydrogen atoms upon contact with hot metal catalyst surfaces such as copper (Cu) and nickel (Ni). The carbon atoms first diffuse through the metal catalyst, and when carbon solubility limit is achieved, graphene sheets are deposited and formed on the catalyst surface (Lee 2012). The first planar few-layer graphene was formed by using camphor as carbon source on Ni foils (Somani et al. 2006). Subsequent studies reported the growth of three to four layers of graphene of 1–2 nm thickness on Ni plates by using hydrogen (H_2), methane (CH_4) and argon gas mixture (Obraztsov 2007; Yu 2008). Further development of CVD under isothermal and isobaric conditions led to the formation of graphene on Cu foils with high quality and uniformity (Li 2009). However, the limited solubility of carbon in Cu results in the self-limiting growth of graphene sheets on Cu foils. A recent study also reported the production of few-layered graphene by using a magnesium oxide (MgO)-supported cobalt

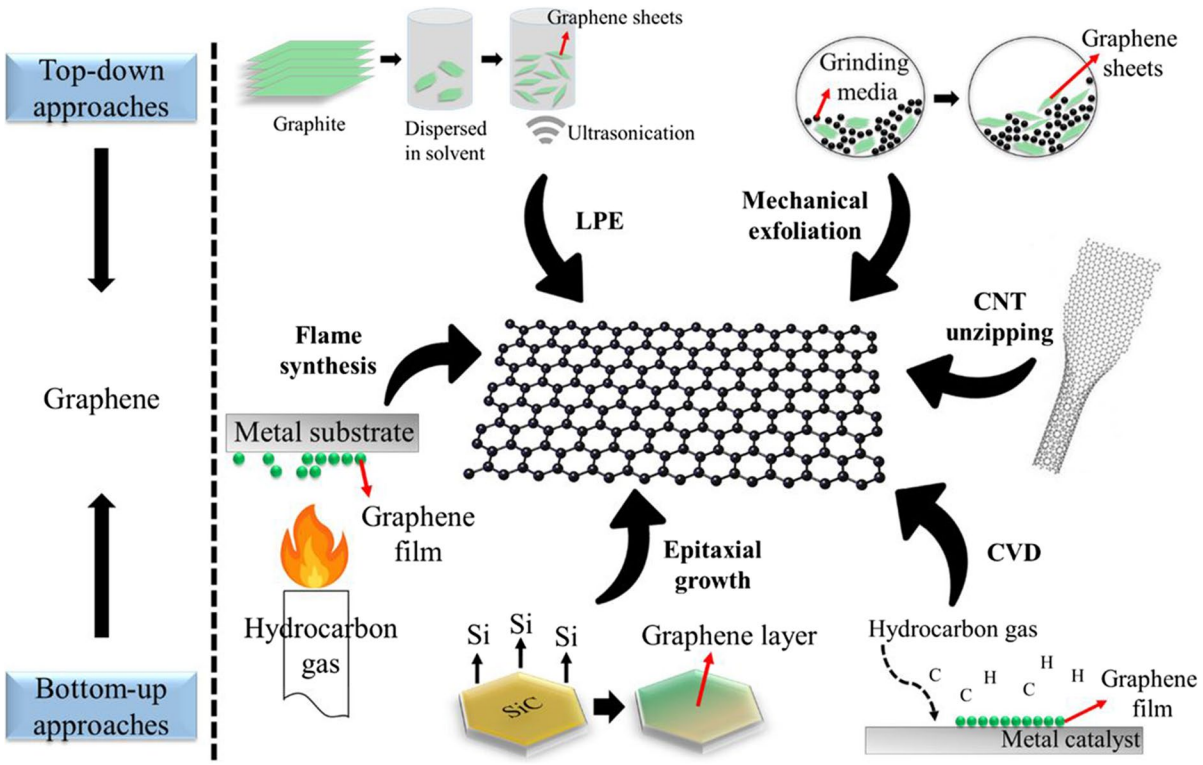

Fig. 1 Examples of conventional bottom-up and top-down approaches for the synthesis of graphene

catalyst to deposit graphene on a ceramic boat (Wang et al. 2009).

Another bottom-up synthesis of graphene is through epitaxial growth, where hexagonal substrate (silicon carbide, SiC) decomposes at 1200–1600 °C under vacuum or inert condition (Mishra, et al. 2016). The high-temperature process results in the sublimation of Si, allowing excessive C atoms to aggregate and induce the growth of graphene. The major drawback of this method is the lack of homogeneity in the growth of graphene; hence, alternate substrates such as polytetrafluoroethylene (Manukyan 2013) and CO_2 laser (Yannopoulos 2012) are employed to ensure the homogeneous growth of graphene.

Flame synthesis is a relatively new production method as graphene film grows on metal substrates in situ and ex situ of a flame in the presence of hydrocarbon gases such as CH_4 and H_2 providing carbon species for growth. Transition metals with high carbon solubility due to their incomplete *d* orbitals are potential metal substrates for the growth of graphene (Memon 2013). The formation of amorphous carbon film was observed on the Cu substrate plate over an ethanol burner (Li 2011a), and similar carbon particles containing graphene were also collected over a propane flame (Ossler 2010). Although a non-oxidative environment is proven to enhance the growth of graphene (Li 2011b), the fluctuating temperature and species gradient present in the flame cause difficulties in scaling up the growth of graphene sheets (Hu et al. 2017).

Top-down approaches

Graphite is essentially stacked layers of graphene bounded by van der Waals forces. Top-down methods such as mechanical and liquid-phase exfoliation of graphite, and unzipping of carbon nanotubes (CNTs), include a series of bond breaking, decomposition of carbon-based precursors and delamination of graphite layers to produce single-layer, bilayer or few-layer graphene (Lee 2019). Early production of graphene was carried out by micromechanical exfoliation of highly ordered pyrolytic graphite (HOPG). The process involves repeated peeling using adhesive tape to cleave HOPG and to produce few-layer graphene with high-quality crystallites ($> 100\ \mu m^2$) (Allen et al. 2010). However, this method is limited to laboratory scale and is not feasible for large-scale production of graphene.

Alternately, liquid-phase exfoliation (LPE) that utilises solvent and ultrasonication for exfoliation has been explored as an alternative. Solvents with suitable surface energy, surface tension and solubility parameter are crucial to overcome the van der Waals forces for effective LPE. The energy required for the exfoliation of graphite is countered by the interactions between solvent and graphene. Solvents or ionic liquids having similar surface energy as graphene, i.e. 70–80 mJ m^{-2}, or surface tension within 40–50 mJ m^{-2} (Lee 2019) are ideal for LPE due to a smaller mixing enthalpy and hence an easier exfoliation process. Typical ultrasonication time for LPE is 1 h, employing a sonication power of 250–500 W (Aissa 2015). Over 40 types of solvents were studied in LPE for the production of graphene (Hernandez 2010), which include water–ethanol/isopropanol (Yi 2012); acetic acid, sulphuric acid and hydrogen peroxide (Singh 2011); sodium cholate (Green and Hersam 2009); hydrazine hydrate (Stankovich 2006); and *N*-methyl-pyrrolidone (Hernandez 2008). The outcomes obtained from these studies suggest low-cost and stable solvents for the production of high-quality graphene. Conversely, mechanical exfoliations based on shear force vectors, such as ball milling, are also applied to produce graphene materials. The mechanical force generated by grinding media via impact and attrition facilitates the exfoliation and fragmentation of graphite to graphene flakes (Yi and Shen 2015), as well as functionalisation of graphene (Fan 2016) and fabrication of graphene composite (Bastwros 2014).

The unzipping of CNTs involves cutting of the cylindrical structure to lay flat the carbon sheets into single-layer, bilayer or few-layer graphene. Single or multiwalled CNTs are used as starting materials where the obtained products with the different numbers of layers are termed as nanoribbons. The unzipping of CNTs generally requires a high strain rate at $10^{8–10}$ s^{-1} to break C–C bonds in the axial or longitudinal direction (Tiwary 2015) which is achievable by means of chemical attack (Kosynkin 2009), plasma etching (Jiao 2009), intercalation and exfoliation (Cano-Márquez 2009) and metal-catalysed cutting (Thess 1996). Although the unzipping of CNTs produces graphene with smooth edges and narrow size distribution typically between 10 and 20 nm (Jiao 2009), issues of low product yield, destruction of a significant amount of precursors and

the usage of aggressive oxidants such as potassium permanganate ($KMnO_4$) and potassium perchlorate ($KClO_4$) (Mondal et al. 2018) have to be resolved for more efficient production.

In general, bottom-up approaches produce near-defect-free graphene materials with large surface areas at the stake of high production cost and complex processing steps. Conversely, top-down approaches are scalable and could possibly produce high-quantity end products; yet the quality, especially the properties, of graphene produced is highly dependent on the finite graphite precursors. Thus, efficient methods for mass production of high-quality graphene are crucial for future industrial implementation.

Graphene synthesis by supercritical fluid exfoliation

Many existing methods for graphene synthesis are held back by the viability to scale up productions without compromising the quality of graphene and its yield, as well as production costs and other possible impacts to the environment. Whilst LPE and conventional chemical oxidation–reduction are considered as more viable approaches for mass production of graphene, the yield and quality of graphene attained is relatively low, and more defects are produced on graphene materials during the reduction process. Therefore, alternative SCF technologies are applied where the tunability of SCF properties could significantly enhance the production of graphene (Rangappa et al. 2011). SCFs have typical properties such as density, solvation, polarity, viscosity and surface tension that fall within those of their gas and liquid states. By adjusting the operating temperature and pressure, SCFs can achieve low interfacial tension, high diffusivity, high compressibility and excellent surface wetting properties (Padmajan Sasikala et al. 2016) that are suitable for graphene synthesis by diffusing in between layers and expand for exfoliation. Conventional SCFs that are commonly used in the process industry include *N*-methyl-2-pyrrolidone (ScNMP) (Rangappa, et al. 2010), *N*,*N*-dimethylformamide (ScDMF) (Liu et al. 2012), water (ScH_2O) (Morales Ibarra, et al. 2020), carbon dioxide ($ScCO_2$) (Xu et al. 2015) and various alcohols (Seo 2013; Nursanto 2011; Zhang 2010). The discussion in this section only focuses on reported works of SCFs as penetrants in intercalating and exfoliating graphite into its 2D form whilst reduction mechanisms of graphene oxide with SCFs are discussed at length in the subsequent section.

Intercalation and exfoliation with SCFs

Exfoliation using SCFs is an extension to LPE where graphite samples are first dispersed in the solvents of choice and subsequently transferred to reactors and heated beyond the supercritical state. SCFs play multifaceted roles in the synthesis of graphene materials, as solvent penetrants, anti-solvents and/or reaction media. In the supercritical state, due to higher solvation power (Rangappa, et al. 2010) as well as diffusion coefficients, the solvent molecules rapidly penetrate through the interlayers of graphite, thus weakening the van der Waals forces of attraction binding the graphite layers (Tao 2017). When $ScCO_2$ is introduced into a graphite–polymer suspension in another solution that is miscible in CO_2, direct exfoliation and synthesis of graphene–polymer composite can be achieved through the anti-solvent mechanism, whereby the injection of $ScCO_2$ weakens the solubility of polymer in the suspension leading to supersaturation and precipitation of polymer onto the graphene layer (Padmajan Sasikala et al. 2016; Zheng 2012).

As such, the choice of SCFs is crucial as the interaction between solvent and graphite layers should be sufficient to offset the van der Waals attraction between graphitic layers, thereby breaking the graphene layers loose (Hernandez 2010). Much work has been devoted to study the interaction between graphene and exfoliating solvents. Through studying the dispersibility and stability of graphene in 40 solvents, Hernandez et al. (Hernandez 2010) discovered and greatly expanded the choice of solvents for graphite exfoliation and other advanced material synthesis and applications. The authors deduced that fundamentally effective solvents are those for which solvent and nanomaterial have the same surface energy, and also related the Hansen solubility parameters (HSPs) of graphene to the Flory–Huggins parameter, a metric used to determine the energetic cost for graphene dispersion and exfoliation, for solvent identification and selection (Hernandez 2010). Wu and Yang (Wu and Yang 2011) studied the interaction of

graphene nanosheets in $ScCO_2$ and calculated the potential of mean force (PMF) between two graphene sheets. The intercalated CO_2 molecules between the graphite layers contributed to a repulsive free energy barrier that prevents graphene from aggregation. The repulsive force is greater at higher $ScCO_2$ density as more CO_2 molecules are entrapped (Wu and Yang 2011). Intercalation of SCF molecules between graphite layers can be expedited through the exertion of external forces via sonication and stirring, or through the addition of molecular wedges such as pyrene and its derivatives (Li 2013). With the expansion of $ScCO_2$, non-covalent functionalisation occurs with the remaining pyrene derivation anchoring on graphene sheets through the π–π interactions, which could be useful for future applications. Apart from graphene synthesis, the roles of SCFs for the synthesis of other 2D materials such as titania and molybdenum disulphide (MOS_2) have been reviewed in other literature (Sun et al. 2019; Padmajan Sasikala et al. 2016). Subsequent exfoliation of graphite is achieved through rapid expansion of supercritical suspension (RESS) by the abrupt release of the mixture from its supercritical state by relieving the reactor content through a nozzle or an orifice, or by rapidly opening the vent valve. The graphite layers expand following the intercalation of solvents, and a sudden depressurisation reverts SCF to its subcritical state, causing large pressure gradients that push the graphite layers apart, thus forming graphene sheets of monolayer to multiple layers depending on the degree of intercalation (Sun et al. 2019; Gao and Hu 2016). Likewise, the exfoliation of graphene can be enhanced through assisted exfoliation with sonication and/or mechanical stirring that induces a higher shearing effect on graphene fractioning.

Types of SCF media

In this section, reported works on direct exfoliation of graphite to graphene are distinguished for various types of supercritical solvents. The roles of SCFs as intercalants and other methods that promote SCF intercalation and exfoliation are reviewed. The properties, advantages and disadvantages of various SCFs are summarised under Table 1.

Supercritical organic solvents

Organic solvents such as *N*-methyl-2-pyrrolidone (NMP) and *N*,*N*-dimethylformamide (DMF) with surface tension close to that of the surface energy of graphene (Amiri 2018) are commonly used in liquid-phase exfoliation of graphene at ambient condition. At supercritical points, the intrinsic solvent properties such as densities and viscosities are tunable (Sun et al. 2019) by altering temperature and pressure, thereby enhancing the solvent intercalation effect. Following successful demonstration of silicate delamination with supercritical CO_2 by Serhatkulu et al. (Serhatkulu et al. 2006), Rangappa et al. (Rangappa, et al. 2010) carried out a single-step direct exfoliation of graphite crystals into sheet form without chemical modification with supercritical fluids such as ScDMF, ScNMP and ethanol (ScEtOH) by first dispersing them into the respective solvents, followed by heating the reaction vessel to achieve a supercritical state. The exfoliation process is as illustrated in Fig. 2 which shows the solvent penetrating through the graphitic interlayers. The conversion successfully yielded about 90–95% of graphene sheets with less than 8 layers, and approximately 6–10% monolayers, whilst the remaining have more than 10 layers. The exfoliation efficiency for the three different SCFs is seemingly comparable. Liu et al. (Liu et al. 2012) used ScDMF with expandable graphite which are pre-intercalated graphite with uneven spaces around them, allowing supercritical DMF molecules to enter easily and rapidly, as starting materials. The exfoliation time with ScDMF was greatly reduced compared to liquid exfoliation that was carried out at ambient condition. However, the use of the aforementioned organic solvents, which generally are toxic and have high boiling points, raised concerns about their impacts on the environment. Thus, researches explored the utilisation of alternative solvents for exfoliation processes (Liu 2019a).

Supercritical alcohols

Rangappa et al. (Rangappa, et al. 2010) successfully repeated direct graphite-to-graphene exfoliation with methanol as a cheaper alternative, yielding graphene sheets with 1 to 10 layers. The graphite flakes were pretreated with dilute sulphuric and nitric acids that facilitated the dispersion of the flakes in methanol. Hadi et al. (Hadi 2016) examined the use of supercritical ethanol as the intercalation agent with water as co-solvent and applied the concept of HSPs to study the exfoliation efficiency. The HSP is a parameter used to determine the surface energy–based

Table 1 Advantages, disadvantages and supercritical conditions of different solvents

Solvent	T_c and P_c	Advantages	Disadvantages	Ref
Carbon dioxide ($ScCO_2$)	32.1 °C, 7.4 MPa	Low supercritical temperature with lower energy requirement Abundant in the industry as it is the by-product of industrial processes and non-toxic	Liquefaction of CO_2 gas is needed for reactor feeding. Disposal of large amounts may contribute to greenhouse gas effects	Bell 2020; Beckman 2004)
Simple alcohols	239–290 °C, 4.4–8.1 MPa	Common in industry Affordable and environmentally preferred	Flammable and corrosive	Rangappa, et al. 2010; Seo 2013; Hadi 2016)
N, *N*-Dimethylformamide (ScDMF)	377 °C, 4.4 MPa	Less pressurisation is needed and hence reduces the risk of explosion	Decomposes at 450 °C, affecting the properties of graphene Harmful through skin contact and inhalation Causes eye irritation More energy is required to achieve the critical temperature	Rangappa, et al. 2010; Information, N.C.f.B. 2004a)
1-Ethyl-2-methyl pyrrolidone (ScNMP)	445 °C, 4.7 MPa	Relatively low toxicity and potential for skin irritation	More energy is needed to achieve supercritical temperature	Åkesson 2001; Information, N.C.f.B. 2004b)

interaction between graphene and exfoliating solvents, where the energy requirement for exfoliation will be lower due to a smaller enthalpy of mixing when the solvent HSP values are close to those of graphene (Cui 2011), thus facilitating a more efficient exfoliation. The authors adopted response surface methodology in the experimental design to study the effect of temperature, pressure and contribution of water as co-solvent on the exfoliation yield, and calculated the HSP for the binary solvents corresponding to the changes of experimental conditions to elucidate the effect of supercritical conditions on graphene exfoliation. By adjusting the supercritical conditions

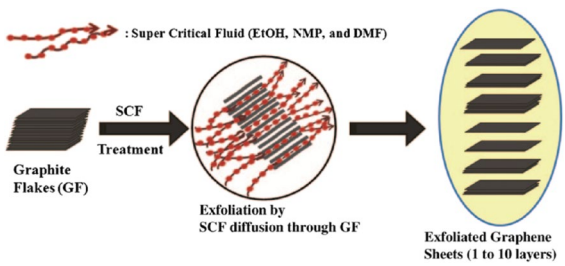

Fig. 2 Direct exfoliation of graphite crystals into graphene sheets with SCFs as an exfoliating and intercalating agent as demonstrated by Rangappa et al. (Rangappa, et al. 2010)

and thus the solvent strength and solubility parameter, the HSPs can be altered according to the affinity between the supercritical fluid and graphene flakes, in which in the use of ScEtOH in this study, an increase in temperature and a decrease in pressure resulted in a monotonical decrease of the HSP values. The results indicated that the highest achievable yield is at 18.5% of monolayer to few-layer graphene with optimum conditions at 325.1 °C and 39.8 MPa with 28.9 wt% of water. The effect of water content variance in the mixture between 0 and 50% to the exfoliation yield is less apparent from the study, thus also suggesting probable replacement of organic solvent with water as a more environmental friendly alternative.

The use of inorganic solvents such as ammonia ($ScNH_3$) has also been reported, whereby nitrogen-doping (N-doping) of graphene occurred simultaneously with exfoliation (Sasikala 2016). Direct exfoliation of graphite with simultaneous N-doping avoids undesired oxygen functionalities. The $ScNH_3$ resultant N-doped graphene demonstrates significantly lesser defects with a higher amount of nitrogen than liquid-phase–exfoliated graphene with ammonia solution (NH_4OH). The $ScNH_3$ graphene also exhibited a better oxygen reduction reaction activity.

Supercritical carbon dioxide

Ibarra et al. (Morales Ibarra, et al. 2020) compared the quality of exfoliated graphene using supercritical CO_2 against supercritical water and ethanol and confirmed the impact of exfoliation. $ScCO_2$ is, by and large, regarded as a green solvent offering a milder and more environmental friendly approach for the synthesis of graphene (Liu 2019a). With a critical temperature and pressure at 31.1 °C and 7.4 MPa, respectively, it is a low energy–consuming solvent as compared to other solvents aforementioned (Zhang et al. 2014). However, owing to its non-polar nature and smaller molecular size (Gao and Hu 2016), the intercalation effect of $ScCO_2$ is less effective than that of organic solvents. Gao et al. (Gao 2017) added an aqueous solution of $EtOH/H_2O$ to the $ScCO_2$ system, which was assisted by ultrasonication. A suspension of graphene sheets in aqueous solution was obtained with graphene yield reaching more than 50%, where 93% of the exfoliated sheets had less than 3 layers.

Supercritical co-solvents, CO_2 expanded solvent and use of surfactants

Liu et al. (Liu 2019a) reported on the application of $ScCO_2$ with NMP for the exfoliation of expandable graphite into graphene, where an increase in the amount of graphene and the rate of few-layer graphene were noted. The suspension of graphite in NMP was fed, and CO_2 was charged into the reactor with magnetic stirring. Molecular dynamic simulations were also carried out to study the effect of $ScCO_2$-NMP on the exfoliation of graphite. The simulation indicated enhanced intercalation of graphite interlayer through the diffusion of CO_2 into the graphite layers supported by the larger NMP molecules as wedging molecules as illustrated in Fig. 3. The expansion of solvents in graphene mixture with CO_2 gas is termed as CO_2-expanded liquids. The latter are another form of tunable solvents with close similarity to that of $ScCO_2$ yet require milder operating conditions. CO_2-expanded liquids demonstrate excellent mass transfer with the addition of a large amount of CO_2 (Xu et al. 2018). The yield of graphene obtained through this method was quite low yet could be further improved with sonication after agitation of the gas-expanded solvent and graphite mixture. Amongst other suitable solvents to be coupled with CO_2 expansion method include ethylene glycol and ethanol (Xu et al. 2018). Graphene derived from exfoliation with $ScCO_2$-assisted organic solvents in suspension form can directly be used for synthesising composite materials (Gao 2017).

Xu et al. (2015) proposed employing surfactant for reverse micelle–induced exfoliation in $ScCO_2$ and demonstrated that using non-ionic polyvinylpyrrolidone (PVP) yielded 87.7% of graphene nanosheets of equal or less than three layers with a concentration of 1.93 mg mL^{-1}. Amongst other surfactants tested (cetrimonium bromide and pluronic), PVP demonstrated the strongest interaction with graphene sheets, attributed to a higher adsorption capability due to the presence of pyrrolidone group. The addition of PVP created a microemulsion environment. The capacitance of the exfoliated graphene was 71.1% higher than that of pristine carbon materials.

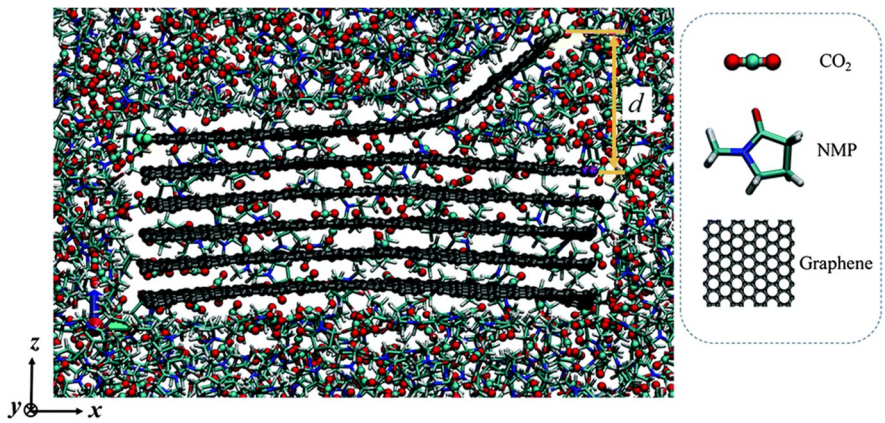

Fig. 3 Atomistic model of $scCO_2$-assisted NMP intercalation built by Liu et al. (Liu 2019a). The MD simulations were performed to elucidate the synergistic exfoliation effect of $ScCO_2$-NMP, and the simulations were set at conditions akin to the experiments conducted

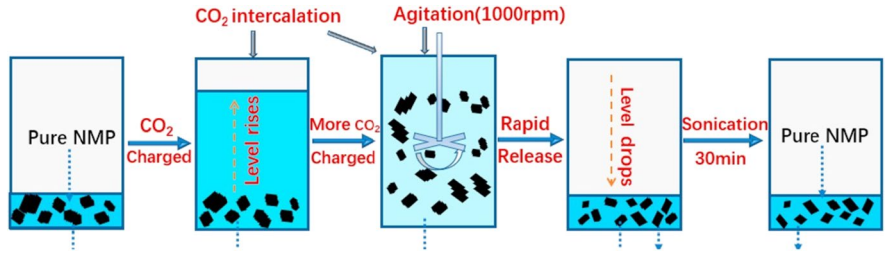

Fig. 4 Schematic flow diagram of a shear-assisted SCF exfoliation of graphite into graphene with NMP as a SCF solvent (Xu et al. 2018)

Assisted exfoliation

As discussed in sections "Supercritical carbon dioxide" and "Supercritical co-solvents, CO_2 expanded solvent and use of surfactants", the exfoliation of graphite with $ScCO_2$ alone may not be efficient enough to obtain a higher yield of few-layer graphene sheets. Hence, the process is commonly coupled with other approaches such as ultrasonication and shear mixing. Xu et al. (2018) first exfoliated graphite flakes using the $ScCO_2$/NMP mixture in a reactor with a three-blade propeller at 1000 rpm. The schematic flow diagram of the exfoliation process is illustrated in Fig. 4. Upon depressurisation, the mixture was subjected to 30 min of sonication for further exfoliation of the previous semi-exfoliated graphite in the process. This study reported an agitation time of 24 h and a high system pressure of 19 MPa to have positive effects on the product yield. A high yield of more than 90% of the product was found to be two- or three-layer graphene, and 12–38% were monolayer graphene (Xu et al. 2018).

In a different study, a 25-mm six and 12-blade stator has also been introduced into a shear mixer-assisted SCF exfoliation process (Fig. 5(a)) (Song et al. 2016). The system utilises the synergistic effect of fluid dynamic force and supercritical fluid to overcome the van der Waals forces for effective graphene production. Shear force in the system is generated as the $ScCO_2$ is forced into the rotor region at high rotational speed. The large velocity gradient of the fluid facilitates the diffusion and penetration of CO_2 molecules into graphite interlayers due to its zero interfacial force and superior transport properties (Fig. 5(b)). As $ScCO_2$ that entered the rotor region is thrown out from the holes of the stator as a result of high centrifugal forces, the velocity and geometric change of the fluid induce cavitation (Fig. 5(c)), followed by the collapse of bubbles. The tensile strength produced from these cavities will act on the surface of

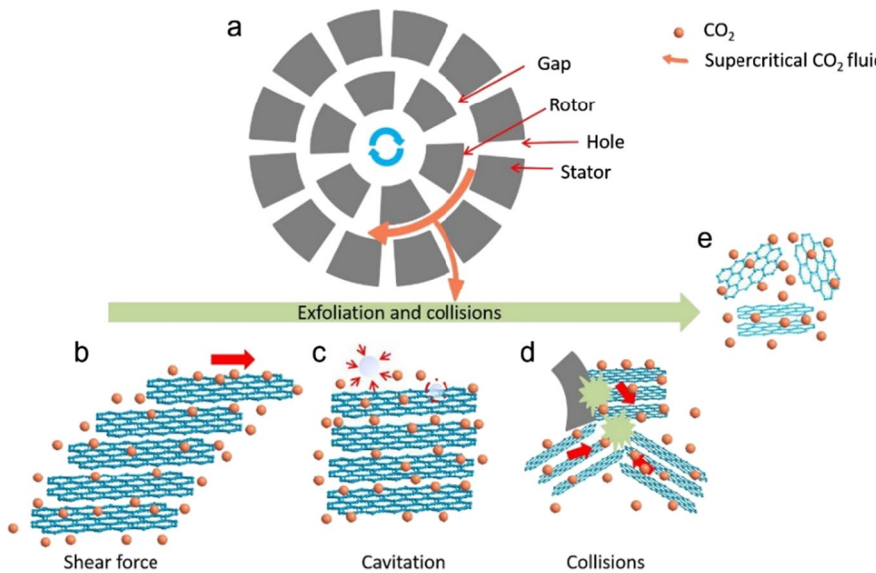

Fig. 5 (**a–e**) Mechanisms of graphite exfoliation by fluid dynamic force in supercritical CO_2 assisted by a six and 12-blade stator (Song et al. 2016)

graphite and exfoliate graphite into graphene sheets. Random and edge collisions (Fig. 5(d)) in the reactor are also reported as possible mechanisms in the fluid dynamic force–induced exfoliation system for graphene production (Fig. 5(e)). The six and 12-blade stator shear mixer reports a graphene yield of 63.2%, with 79% of the produced graphene is less than 5 layers, amongst which the trilayer, bilayer and monolayer fractions are 14%, 25% and 27%, respectively.

Higher efficiency in the exfoliation of graphene was observed when the expansion–exfoliation process was coupled with ultrasonication and shear mixing. Whilst some researchers have suggested that enhanced exfoliation is due to the cavitation bubbles generated during sonication which upon collapse release energy that could induce exfoliation, Gai et al. (2018) and a few other authors raised doubts on this possibility especially in the case of $ScCO_2$ where phase boundaries are non-existent above the critical point (Kuijpers 2002), and instead proposed alternative mechanisms. Computational fluid dynamics (CFD) simulations were carried out to study the effects of process parameters and their contribution to the exfoliation yield of graphene, as well as to verify the cavitation phenomena in $ScCO_2$ supported by other authors (Gai et al. 2018). Gai et al. (2018) deduced that the primary factors that promote exfoliation in an ultrasound-assisted $ScCO_2$ exfoliation process are due to the shear stress generated by the acoustic waves and pressure fluctuation in the fluid which cause compression and expansion of the intercalated CO_2, thereby increasing exfoliation. An increase in the system pressure indicates the generation of more energy and facilitates exfoliation. Yet, upon exceeding the optimum conditions, the yield decreases as high pressure starts counteracting the effect of ultrasound with a sharp decrease in CO_2 density.

Wang et al. (2018) reported on the coupling of ultrasound and shear mixing with $ScCO_2$ which produces a synergistic effect on the production of graphene up to 82.6%, with about 60% graphene sheets having fewer than three layers. Ultrasound contributed to higher partial energy in SCF, which may be sufficient to exfoliate the graphite edge partially. In contrast, a high shear force is created from the rotational movement of the mixer rotor, which effectively peels off graphene sheets with active edges. Repeated exfoliation process under the same conditions increased the overall yield (Sim 2012). Similarly, graphene sheets with reduced thickness and lateral size are obtainable through intermittent heating and cooling, believed to be resulting from the thermal shock arising during rapid heating and cooling (Tomai et al. 2012).

Sizing and characterisation of graphene

The size of graphene sheet is crucial for the production and application of graphene-based materials (Liu 2019b) where exfoliated sheets generally have reduced thickness and lateral dimensions (Hadi 2016). Ibarra et al. (2020) compared the exfoliated products with $ScCO_2$, ScH_2O and ScEtOH graphenes. They noticed ScH_2O-exfoliated graphenes have the largest lateral size of around 5 µm whilst ScEtOH graphenes were highly dispersed in the exfoliation medium with the smallest size recorded.

Raman spectroscopy

Raman spectroscopy is used to determine the exfoliation effect by identifying the number of layers, structure and graphene disorders (Rangappa, et al. 2010). Figure 6 shows the Raman spectra of graphite and $ScCO_2$-exfoliated graphene assisted by shear mixing (Song et al. 2016) and the enlarged 2D band regions for graphene of monolayer, bilayer and multilayer. In particular, the G and 2D Raman peaks change in shape, position and relative intensity with the number of graphene layers (Ferrari 2007), with the G band at 1580 cm^{-1} explaining the in-plane vibration of sp^2 carbon atoms. A characteristic shift in the 2D band towards a smaller Raman number as well as a sharper 2D peak confirmed the exfoliation of graphite into graphene (Morales Ibarra, et al. 2020). The D band at 1350 cm^{-1} indicates the structural disorder or edge defects in graphene, wherein an apparent peak at the D band characterises the edge arrangement as armchair-edged, as opposed to perfect zigzag arrangement in the absence of the D band, which is uncommon (Jorio et al. 2011). The intensity ratio of D band to G band (I_D/I_G) characterises the degree of graphitisation, where a lower I_D/I_G ratio signifies more graphitic layers and fewer defects (Wu 2012). Notably, the exfoliated graphene sheet has a higher I_D/I_G value which could be attributed to the increase of boundary edges (Liu 2019a). Nonetheless, the calculated

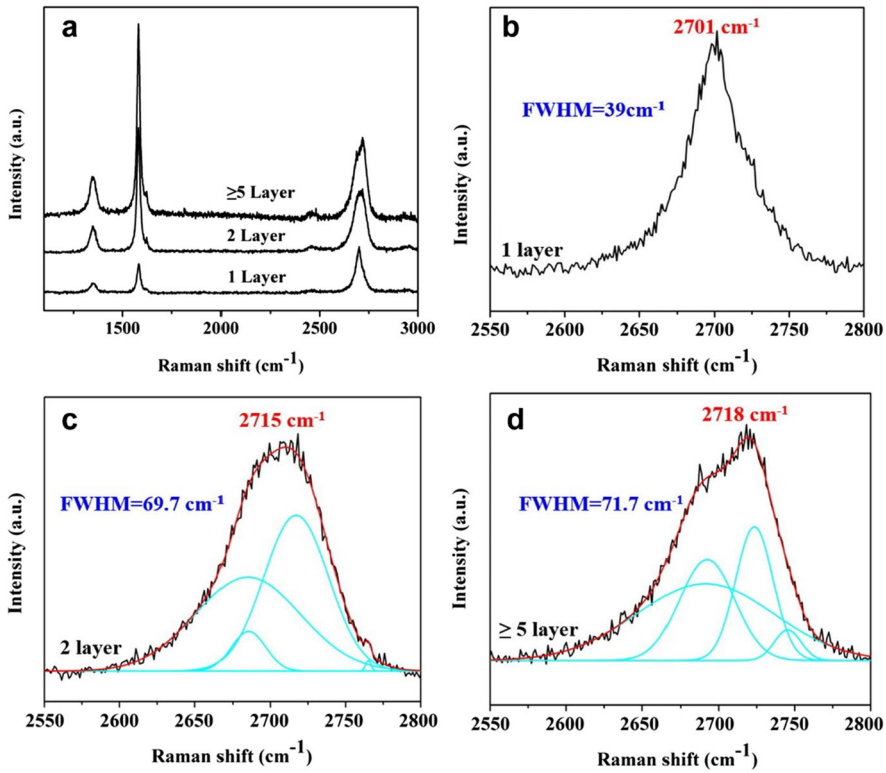

Fig. 6 (**a**) Raman spectra of shear mixing–assisted graphite-to-graphene exfoliation with $ScCO_2$ for graphenes of monolayer, bilayer and more than or equal to five layers. (**b–d**) Enlarged 2D band regions of graphene with curves fitted by Lorentzian functions for graphenes of monolayer, bilayer and more than or equal to five layers, respectively (Song et al. 2016)

I_D/I_G ratio is not conclusive of the edge orientation, whether it is armchair or zigzag orientation without an accurate analysis of the polarisation dependence of the incident light (Casiraghi 2009). The full width at half maximum (FWHM) of the band peaks is also used to quantify the disorder especially interdefect distance, where FWHM increases with disorder (Jorio et al. 2011) as well as the number of layers (Karamat 2015). A major discrepancy is noted in the 2D FWHM of $ScCO_2$-exfoliated monolayer graphene at 39 cm^{-1} in Fig. 6b when compared to other literature suggesting typical 2D FWHM from 25 to 30 cm^{-1} for free-standing monolayer graphene and monolayer graphene synthesised through CVD (Karamat 2015; Berciaud 2009). Yet, the results obtained by Song et al. (2016) appear to be in agreement with other reported FWHMs of 2D peaks for monolayer and disoriented bilayer graphene formed through CVD on copper catalyst, at 37 cm^{-1} and 27.4–38.2 cm^{-1}, respectively (Liu 2012). As such, meaningful interpretation of the Raman spectra, especially the 2D band when determining the number of graphene layers, should also be coupled with other characterisation to validate the experimental yield.

Atomic force microscopy (AFM)

Atomic force microscopy (AFM) is used to determine the size and thickness of the exfoliated graphene sheet against a substrate, usually mica (Lee and Park 2019). Whilst the application of AFM for the determination of the thickness of single-layer graphene has resulted in variations from 0.4 to 1.7 nm, the observed disparity is attributed to factors such as interactions between the AFM probe tip and graphene as well as due to the ambience at which the materials are prepared (Shearer 2016). Nonetheless, AFM is still one of the most powerful tools for analysing graphene, and the results are often verified with other characterisation techniques such as Raman spectroscopy for the approximation of the number of graphene layers. Figure 7 shows the AFM images obtained by the exfoliation of graphite with $ScCO_2$-assisted NMP along with the corresponding height and length profiles (Liu 2019a). The calculated height for the exfoliated graphene nanosheets ranges from 0.49 to 3.87 nm, suggesting graphene sheet thickness of 1–8 layers. A comparison was also drawn on the exfoliating effect of pure $ScCO_2$ and ScNMP against $ScCO_2$-assisted

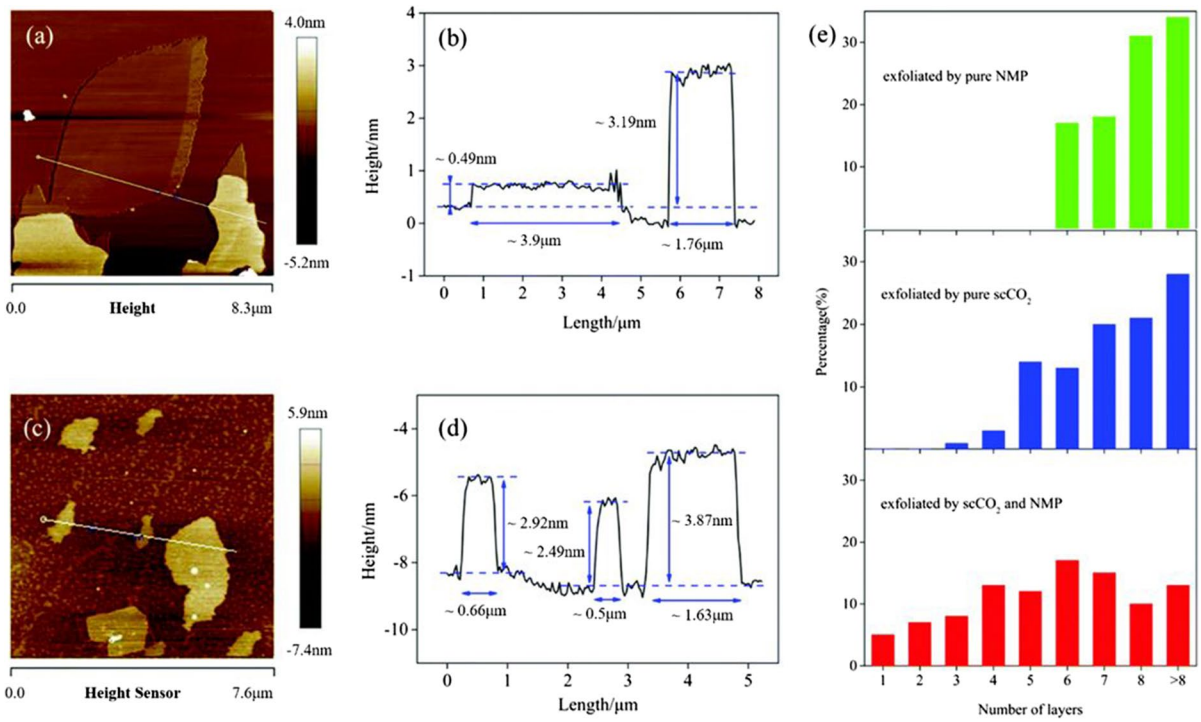

Fig. 7 (**a**, **c**) AFM images of $ScCO_2$-assisted NMP-exfoliated graphene. (**b**, **d**) Measurements and profiles of height and length of graphene corresponding to lines shown in **a** and **c**. **e** Distribution of the resulting layer numbers of graphene exfoliated through different methods (Liu 2019a)

NMP exfoliation, where a higher yield of fewer layers was obtained as shown in the layer number distribution (Fig. 7e). A yield of over 85% of 1–8 exfoliated layers was achieved for $ScCO_2$-assisted NMP, amongst which 30% were graphene with 4 or fewer layers, as compared to a lower yield of less than 70% obtained with pure CO_2 and NMP. The synergistic effect of $ScCO_2$-NMP exfoliation was investigated through MD simulation as illustrated in Fig. 3 in the previous section, which suggested a two-stage diffusion-wedging process during the exfoliation, of which the $ScCO_2$ molecules first diffused into the graphite interlayers, followed by the wedging in of the NMP molecules which enhanced the intercalation effect therein improved the exfoliation of graphene (Liu 2019a). The MD simulation also indicated an overall lower PMF favouring exfoliation when a mixture of NMP and $ScCO_2$ was used, especially at an optimal molecule ratio of 1:1, as compared to that of higher PMF for pure $ScCO_2$ or NMP, thus explaining a lower exfoliation yield when only pure solvents of either are used. Also, as the experiment was carried out at conditions below the supercritical state of NMP, the exfoliated graphene is at least 5 layers thick.

Graphene synthesis by supercritical fluid reduction

Reduction is one of the commonly applied methods for the synthesis of graphene. Conventional approaches utilise strong oxidants to exfoliate graphene oxide (GO) from graphite, followed by the graphitisation of GO into reduced graphene oxide (rGO) by removing the oxygen functional groups and restoring the carbon networks. Oxygenated functionalities, i.e. hydroxyl and epoxide groups on the basal planes and carbonyl and carboxylic groups at the edges (Lerf 1998; Szabó 2006; Bagri 2010), modify the sp^2-bonded carbon network in the initial oxidation step during graphene production. These modifications form a variety of defects, thereby resulting in the degradation of graphene properties (Seo 2013). Thus, reduction methods such as thermal annealing (Mao

et al. 2012; Compton and Nguyen 2010) and chemical reduction (Chua and Pumera 2014; Dreyer et al. 2014) are introduced to recover the disrupted sp^2-conjugated graphene network. Although the thermal annealing process produces graphene-like films with high carbon-to-oxygen ratio and a minimal amount of defects, the higher reaction temperature (above 1000 °C) limits the types of starting materials compatible with the reaction condition (Kong 2012).

Similarly, chemical reduction processes apply reducing agents such as hydrazine (Tung 2009), sodium borohydride (Shin 2009) and sodium borohydride with concentrated sulphuric acid (Gao 2009), which are highly unstable, toxic or explosive for the reduction of GO at lower temperatures (below 100 °C). Effective removal of oxygen functionalities (C/O ratio ranges from 8 to 15) and high electronic conductivity (5000 to 30,400 S m^{-1}) are achieved by using such strong reducing agents (Seo 2013). However, the extended reaction time and safety concerns which arose from chemical reduction hindered the feasibility of such method in mass production. Thus, supercritical fluid has been explored as an alternative green solvent for the effective removal of oxygen functionalities and the restoration of the unique hexagonal structure in graphene for a more sustainable reduction process.

Graphene reduction by SCFs

Supercritical fluids exhibit great potential in offering an alternative greener route as against using toxic reducing agents and have been employed in the reduction of GO for the production of graphene-like sheets. The controlled deoxygenation of GO under supercritical water (ScH_2O) was studied via spectroscopic analysis under a range of conditions, i.e. 99.85–379.85 °C and 0.04–22.75 MPa (Mungse 2014). The results from spectroscopic analysis report plausible mechanisms for the deoxygenation of GO in the presence of ScH_2O as illustrated in Fig. 8 are as follow: (1) the dehydration of GO initiated by hydrogen ions due to intermolecular or intramolecular reactions under supercritical conditions, (2) the reduction of epoxide or carbonyl groups to form π bonds and (3) decarboxylation to eliminate CO_2 molecules.

The dehydration process can take place between closely placed hydroxyl groups (Fig. 8, positions 1 and 2), hydroxyl groups having adjacent hydrogen atom (Fig. 8, position 3) or between hydroxyl groups of different nanosheets (Fig. 8, position 4) (Mungse 2014). Closely placed hydroxyl groups eliminate water molecules by generating either ether or epoxide linkages, depending on their position in the skeleton. Similarly, hydroxyl groups also remove water molecules by forming olefinic bonds with adjacent hydrogen atom. The dehydration of hydroxyl groups between two different nanosheets generates ether linkages and would result in layer aggregation.

Reduction occurs as the highly strained epoxide groups at the basal plane of GO are reduced to hydroxyl groups due to the presence of nearby hydrogen atom, thus resulting in the formation of π bonds (Fig. 8, position 5). Carbonyl groups are also reduced to hydroxyl groups by generating olefinic bonds during the treatment processes (Fig. 8, position 6). On the contrary, decarboxylation generally involves the removal of CO_2 molecules by consuming carbon atoms (Fig. 8, position 7) or carboxyl group (Fig. 8, position 8) from the GO skeleton at increasing hydrothermal temperature. The aforementioned chemical and structural transformations of GO during reduction exercise restore the conjugated π bonds and stabilise the final graphene structure (Mungse 2014). The thermally unstable hydroxyl and epoxide groups are reduced whilst the comparatively stable ether and phenol groups emerge during the process. As the heteroatom linkage (C–O) of water occurs most readily at high temperature and pressure, the degree of deoxygenation at elevated temperatures (199.85–379.85 °C) was reported to be higher as compared to moderate temperature (99.85 °C) (Mungse 2014).

A recent study incorporated the reduction of few-layer GO (FLGO) and glycerol gasification in ScH_2O, where the deoxygenation of FLGO and valorisation of glycerol catalysed by FLGO could be achieved simultaneously (Torres 2017). The thermal processing of oxygenated organic compounds such as glycerol involves complex chemistry (Wang et al. 1996); thus, a general gasification reaction involving main products is represented in Fig. 9. As the reduction of FLGO consumes intermediate hydrogen (H_2) gas, the gasification reaction is displaced further towards the formation of carbon monoxide (CO), CH_4, more H_2 products and valuable hydrocarbons such as alkylated and non-alkylated long-chain hydrocarbon (C12–C31), polycyclic aromatic hydrocarbons (PAHs), phthalate, phenol, cresol and furan-based

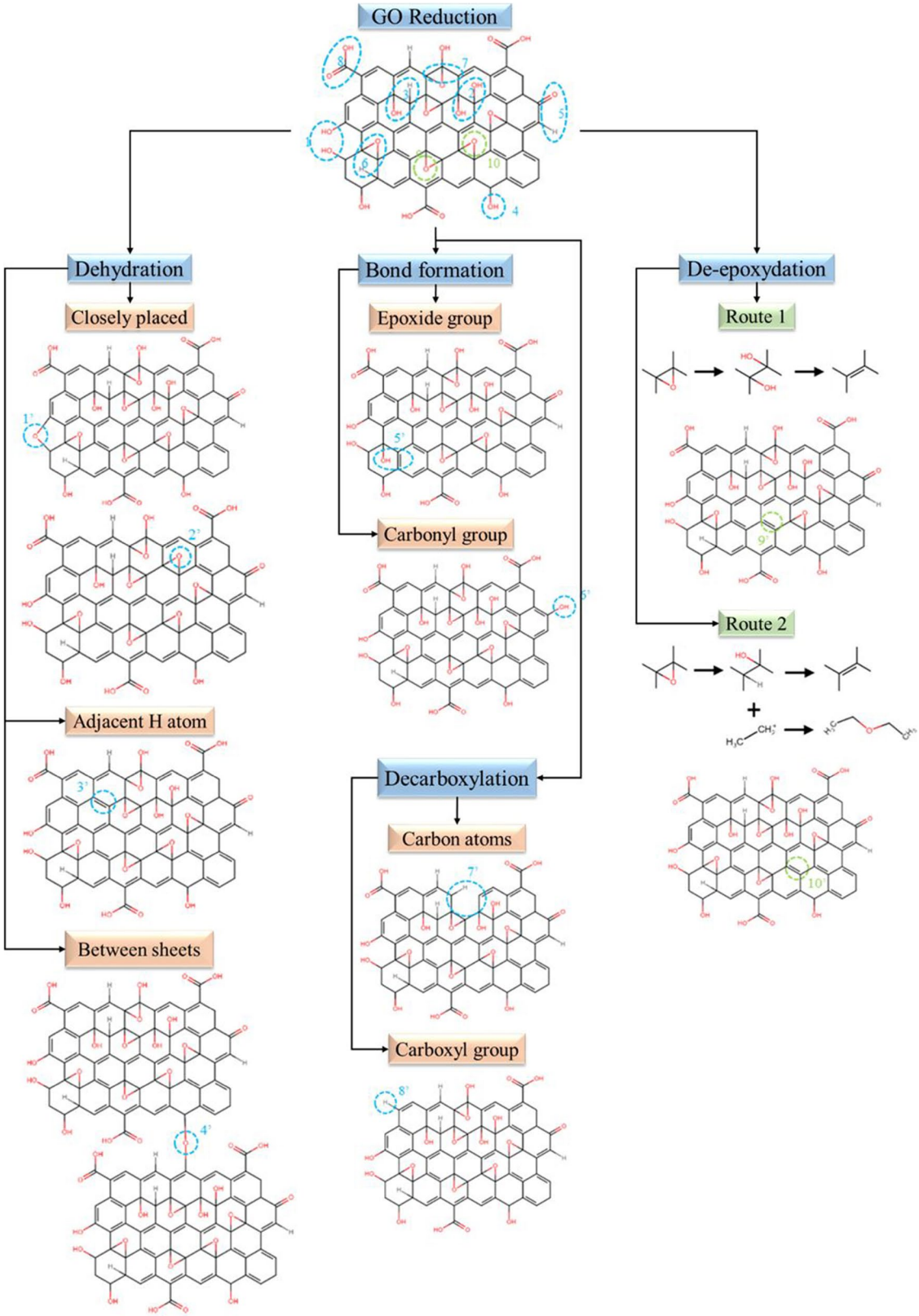
GO Reduction
Dehydration
Closely placed
Adjacent H atom
Between sheets
Bond formation
Epoxide group
Carbonyl group
Decarboxylation
Carbon atoms
Carboxyl group
De-epoxydation
Route 1
Route 2

◂ **Fig. 8** Plausible mechanisms of GO reduction with ScH_2O (Mungse 2014) and ScEtOH (Seo 2013) based on dehydration, bond formation, decarboxylation and de-epoxydation of hydroxyl, carbonyl and carboxyl groups in graphene

compounds in the presence of FLGO. Similarly, glycerol enhanced the generation of in situ hydrogen and improved the removal of oxygen up to 59%, resulting in a final C/O ratio of 28.2 in rGO. Supercritical carbon dioxide ($ScCO_2$) was also used to obtain rGOs by annealing GO at 10 MPa and a maximum temperature of 300 °C (Kong 2012). The study reports on the optimum conversion at 200 °C and a reduction time of 3 h. The electrical conductivity of rGOs annealed in $ScCO_2$ is comparable to those obtained from hydrazine hydrate reduction (Stankovich 2006).

As different supercritical alcohols have a distinctive number of alcohol molecules and hydrogen donating abilities, the produced rGOs are expected to exhibit different physiochemical properties. The performances of different alcohol reductions of GO are summarised in Table 4. Study showed that reduction of GO has been successfully carried out in supercritical methanol (ScMeOH) without using external reducing agents (Nursanto 2011). Similarly, the superior hydrogen donating ability of supercritical ethanol (ScEtOH) under high-pressure and temperature conditions facilitates the restoration of original pristine graphene structure (Rangappa et al. 2011), where the electrical conductivity of rGO produced from ScEtOH reduction was reported to plateau at 250 °C. This confirms the restoration of π conjugation, and intrinsic properties of graphene under alcohol treatments are more significant than $ScCO_2$ reduction (Kong 2012). The C/O ratio and electrical conductivity from both alcohol treatment studies are comparable to those produced by hydrazine reduction methods. Subsequently, in a recent study, the reduction of GO by five alcohols under supercritical conditions (Seo 2013), i.e. ScMeOH, ScEtOH, 1-propanol (ScPrOH), 2-propanol (Sc2IPA) and 1-butanol (ScBuOH), were investigated. A significant difference in the C/O ratio was observed where the ratios in rGO are in the order of ScEtOH > Sc1PrOH > Sc2IPA > ScBuOH > ScMeOH, suggesting that ScEtOH exhibited the most efficient reduction amongst the studied alcohols. The highest C/O ratio (14.4) of rGO produced from ScEtOH treatment may be associated with a larger amount of alcohol molecules in the supercritical state that permeate into the interlamellar structure of GO. The inherent low reduction power of ScMeOH and lower ability to donate hydrogen compared to other supercritical alcohols could have resulted in the lowest reduction efficiency (Ross and Blessing 1979; Nakagawa 2003). In addition, the electrical conductivity of rGO obtained from ScEtOH reduction was reported to be 2.5 times higher than ScMeOH reduction (Nursanto 2011).

The presence of different oxygen functionalities at GO sites, i.e. epoxy and hydroxyl groups are mainly located at the basal plane whilst carbonyl, carboxyl and ester groups are located at the edge and vacancy sites (Lerf 1998; Szabó 2006; Bagri 2010), further complicates the reduction chemistry of GO. Supercritical alcohols retain unique properties that are different from other supercritical fluids in a way where hydrogen is donated in the form of molecular hydrogen, hydride or protons (Seo 2013). The reduction mechanism of GO in alcohol was studied by using ScEtOH, alcohol with superior reduction ability as compared to other alcohols (Seo 2013), and two dominant deoxygenation routes were proposed. Route 1 describes that carbon of the epoxy ring is attacked by both α-hydrogen and hydroxyl groups produced from ScEtOH. The addition of proton and the restoration of π conjugation take place subsequently, resulting in the formation of $CH_2=CH_2$ (Fig. 8, position 9) and two water molecules as by-products. Conversely, hydroxyl functionalities and ethoxy groups are generated as a result of proton transfer from ScEtOH to the epoxy ring in route 2. The hydroxyl groups undergo dehydration to yield olefins and water molecules as by-products whilst the ethoxy groups may also react with $CH_3CH_2^+$ from ScEtOH to yield diethyl ether (Fig. 8, position 10). The observed hydrogen consumption and water or CO_2 formation during ScEtOH reduction can henceforth be taken as the sign of GO deoxygenation.

Reduction of graphene composite by SCFs

The presence of oxygen-containing functional groups in GO provides large surface area and numerous nucleation centres to load nanoparticles (NPs). The combination of GO and NPs could create synergetic effects and exhibit exceptional

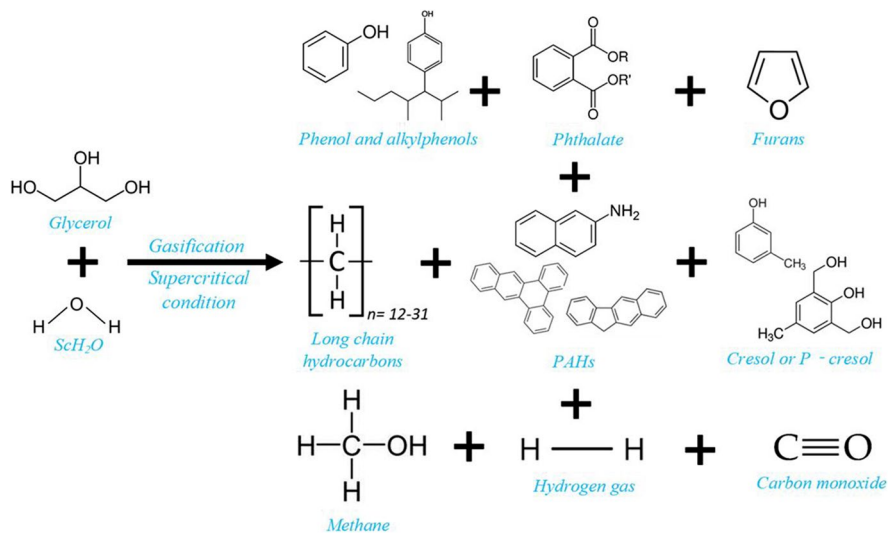

Fig. 9 ScH_2O gasification of glycerol to rFLGO, producing CO, CH_4, H_2 and various valuable hydrocarbons

properties that could not be provided by their individual components. Reduction assisted by supercritical fluids has been applied for the preparation of graphene composites. The unique zero surface tension of SCF is beneficial for substrate wetting and consequently facilitates the adsorption of particles on the surfaces with oxygen functionalities. Electrostatic attraction due to opposite charges between substrates and surfaces drives interlamination to form graphite sheets. Substrates preferably adsorb, decompose, nucleate and grow into NPs on sites containing oxygenated functional groups. The in situ formation of particles destroys and prevents the restacking of regular layers, thus producing graphene sheets containing NPs. Nanocomposites fabricated by $ScCO_2$ technique generally exhibit more well-defined microstructures and macroproperties (Chen 2011; Zhao 2012; Liu and Han 2009).

Nanocomposite of graphene anchored with silver nanoparticles has been successfully produced by $ScCO_2$ chemical reduction (Meng et al. 2016). The C/O ratio of silver–graphene composite fabricated via $ScCO_2$ reduction (SAg/GN) is higher (4.5) than the normal chemical reduction of silver–graphene composite (Ag/GN) (2.3). The oxygen-containing groups decompose in the range of 100–300 °C as $ScCO_2$ transfers more silver nitrate precursors onto the graphene surface. The uniform distribution of silver particles across SAg/GN as compared to the cluster appearance of irregular silver particles on Ag/GN reiterates the exceptional reduction and dispersion ability of $ScCO_2$ on the production of graphene composites. The SAg/GN nanocomposites, synthesised as lubricant additives in engine oil, exhibited remarkable anti-wear abilities as superior to pure engine oil and significantly improved the lubricating performance.

Cobalt tetraoxide (Co_3O_4)/graphene oxide composites were fabricated for catalytic applications with the aid of $ScCO_2$ (Zhao 2014). The average size of Co_3O_4 NPs (5.9 nm) on the composite is smaller than that of bare Co_3O_4 NPs, indicating that the $ScCO_2$-aided process could hinder the growth and prevent aggregation of NPs during the fabrication process. The C/O ratio of the composite was estimated to be 2.9, with notable improvements in catalytic performance by decreasing the decomposition temperature and enhancing the overall exothermic heat release during the chemical process. Similarly, platinum (Pt) precursors were reduced to Pt NPs and were evenly distributed on Pt/graphene composite by using $ScCO_2$ (Zhang et al. 2014). The mean size of Pt particles was 3.28 nm, and again likewise, an enhanced electrocatalytic effect of Pt/graphene composite of 3.5 times higher than that of conventional Pt/carbon black catalyst was observed.

A binary system of $ScCO_2$ and near-critical ethanol was developed to produce rGO–polyethylene glycol (rGO-PEG) films and rGO–polyvinyl alcohol (rGO-PVA) fibres (Sasikala 2018). It is to be noted that ethanol is soluble in $ScCO_2$ and $ScCO_2$ has higher diffusive power. The binary system anticipated that $ScCO_2$ assists ethanol in diffusing into the

polymer matrix volume where ethanol in the interlayers reacts with neighbouring oxygenated groups such as carbonyls or ethers to reopen the hexagonal carbon ring for further carbon incorporation. This reaction allows the removal of oxygenated groups and fosters graphitisation to maintain the homogeneity of GO-PVA films. The presence of graphene network in the polymer matrix is found to enhance the electrical conductivity of the composite significantly. Despite notable improvement in the electrical conductivity was observed with the increase in GO wt% and reduction time, the composite was found to be brittle beyond a reduction time of 2 h. This degradation in mechanical stability is believed to have resulted from the increased crystallinity.

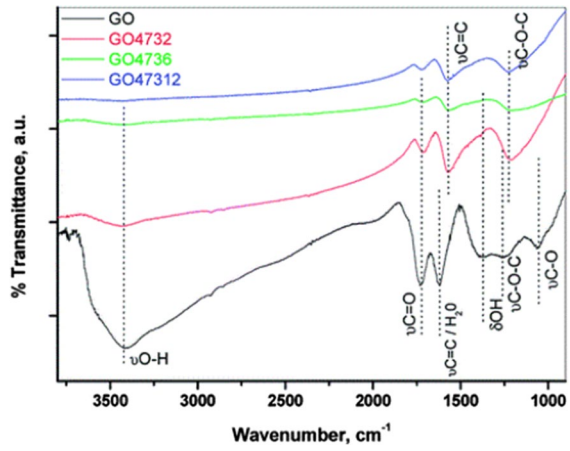

Fig. 10 FTIR spectra of GO and rGO obtained by ScH_2O over 2 h (GO4732), 6 h (GO4736) and 12 h (GO47312) (Mungse 2014). Reproduced with permission

Doping of heteroatoms on graphene sheets with SCF reduction

Considerable studies have shown that graphene doped with heteroatoms such as nitrogen (Qu 2010); aluminium (Jeon 2017); chloride, bromide and iodide (Jeon 2013); and phosphorus (Cruz-Silva 2009) exhibit significant improvements in electrochemical activity, selectivity and durability. Heteroatoms with atomic mass and size similar to carbon allow electrons or holes to be injected easily on the graphene materials, thereby altering the electronic or transport properties of doped materials. A one-pot synthesis technique using $ScCO_2$ demonstrated the production of boron-doped rGO by selecting borane–tetrahydrofuran as the reducer (Zhou 2015). The hierarchically porous structure observed in B-rGO prepared by borane–tetrahydrofuran may be contributed by the reduction of borane and the diffusion of $ScCO_2$. The high degree of reduction (C/O ratio at 5.9) and high surface area in boron-doped rGO show an elevated catalytic activity towards oxygen reduction reaction which are comparable to commercial Pt/C catalyst, but with added durability and resistance to the crossover effect.

Nitrogen (N) (Suresh Balaji et al. 2018) and sulphur (S) (Balaji 2019) heteroatoms were doped onto graphene sheets with the assistance of ScH_2O to enhance the supercapacitive behaviour for fuel cell applications. The obtained results showed that the performance of fuel cell was improved by doping graphene with 2–4.5 wt% of heteroatoms. This enhances the energy density in the ionic liquid electrolyte, thus resulting in superior capacitance retention of 90% over 10,000 cycles. Similarly, the preparation of GO–polyaniline nanocomposite using $ScCO_2$ also exhibits excellent electrochemical capacitance and cycle stability in energy storage applications (Xu et al. 2012).

Characterisation of SCF-reduced graphene materials

The characteristics of graphene materials produced via reduction such as the presence/absence of functional groups, the atomic composition, structural defects and surface area are commonly characterised by a list of analytical equipment. These include, but are not limited to, Fourier transform infrared spectroscopy (FTIR), X-ray photoelectron spectroscopy (XPS), Raman spectroscopy, Brunauer–Emmett–Teller (BET) analysis and high-resolution transmission electron microscopy (HRTEM).

Fourier transform infrared spectroscopy (FTIR)

The functional groups on the surface of graphene materials are characterised by FTIR analysis. FTIR spectra of GO revealed a broad vibration peak at 3415 cm^{-1} attributed to O–H stretching of hydroxyl and phenolic groups; a peak at 1725 cm^{-1} represents the C = O stretching of carboxyl and carbonyl groups, and the peak at 1620 cm^{-1} is associated with trapped

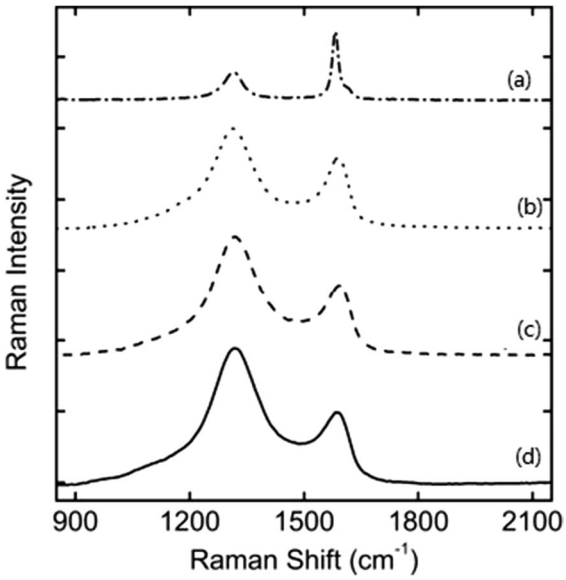

Fig. 11 Raman spectra of the graphite samples (**a**) and ScEtOH-treated rGO (**b**), $ScCO_2$-treated rGO (**c**) and GO (**d**) films (Kong 2012)

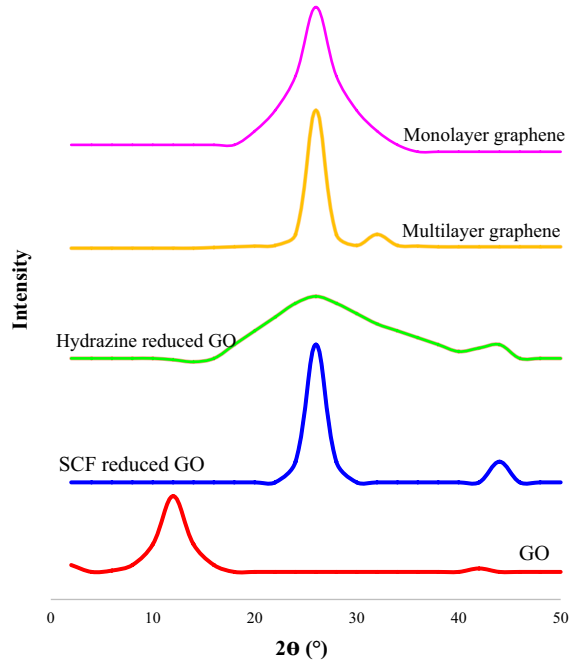

Fig. 12 XRD spectra graphene, rGO treated with hydrazine and supercritical fluid and graphene oxide (Rangappa et al. 2011; Andonovic 2015; Tuz Johra et al. 2014)

water molecules and C=C stretching of unoxidised sp^2 carbon domains in GO (Mungse 2014).

The unresolved broad peak at 1270–1210 cm^{-1} in rGO could be attributed to the C–O–C stretching of epoxy and ether groups which are relatively stable and hindered the complete deoxygenation. The reduction aided by ScH_2O leads to effective reduction within 2 h, and C=C stretching increased significantly as compared to 6 h of deoxygenation, as illustrated in Fig. 10 (Mungse 2014). RGOs produced by reduction utilising different supercritical alcohols exhibit similar FTIR spectra. The intensity of the oxide group transitions in GO decreased after the process; i.e. hydroxyl, carbonyl and epoxide groups attached to the basal layer decreased and a new absorption peak at 1620–1700 cm^{-1} attributed by the skeletal vibration of rGO sheets were observed (Seo 2013; Nursanto 2011).

Raman spectroscopy

The structural and electronic properties of graphene materials such as disorder and defect structures, defect density and doping levels are monitored by Raman spectroscopy. GO generally exhibits graphitic lattice (G) band at 1604 cm^{-1} and disorder (D) band at 1354 cm^{-1} (Kudin 2008). The shift of G band towards lower wavenumber reveals the recovery of hexagonal network (sp^2 carbon domains).

The decrease in the I_D/I_G band ratio of rGO samples is not significant when processing was carried out with $ScCO_2$, indicating that the defects responsible for D band are not sensitive to $ScCO_2$-assisted annealing (Kong 2012).

The rGO sheets reduced under SEtOH exhibit a weak and strong D band at 1326 cm^{-1} and 1576 cm^{-1}, as illustrated in Fig. 11. The increase in I_D/I_G intensity ratio compared to pristine graphite (Rangappa et al. 2011) indicates the decrease in the in-plane sp^2 domain. A repeat of the above experiment with hydrazine reduction confirmed that the intensity ratio of rGO is less significant, suggesting that SEtOH reduction could better facilitate the restoration of original graphene structure owing to the unique properties under SCF conditions.

The Raman spectra of SAg/GN did not show any peaks at 1000 cm^{-1}, indicating the absence of metallic oxide impurities in the composite (Meng et al. 2016). The I_D/I_G ratio of the composites and doped graphene materials was also recorded within the

range of 0.95–1.44 (Sasikala 2018; Suresh Balaji et al. 2018; Balaji 2019).

X-ray diffraction (XRD)

Trapped water molecules and oxygen functionalities within the basal planes of GO result in high interlayer spacing (*d* spacing) and reflected a peak at $2\theta = 10–10.8°$ in the X-ray diffraction (XRD) pattern as illustrated in Fig. 12 (Kong 2012; Mungse 2014; Torres 2017). ScH_2O-treated rGO exhibits peak broadening and a shift of peak to 24–26.3° (Mungse 2014; Torres 2017), indicating the reduction of interlayer spacing and the elimination of oxygen functionalities. However, the restacking of graphene layer due to strong π–π interactions leads to an increased number of layers in reduced FLGO (rFLGO) from 4 to 10 layers, thus exhibiting a similar XRD pattern as multilayer graphene. XRD results for the conversion of rGO from $ScCO_2$ treatment are consistent with the conversion of GO where the common peak at 10° disappears. The absence of graphitic peak suggests that graphitic platelets are not found in $ScCO_2$-treated rGOs (Kong 2012).

The interlayer distance between ScMeOH-treated rGOs was found to decrease from 0.779 to 0.356–0.359 nm whilst the broad peak retained by GO at 11.32° was shifted to 24.74–25° after ScMeOH reduction (Nursanto 2011). A similar observation in the shift of peak position was also recorded in the rGO sheets fabricated with ScEtOH-assisted reduction (Rangappa et al. 2011), revealing the restoration of original pristine graphene structure. An interlayer spacing of 0.358–0.381 nm was recorded for rGO reduced by different supercritical alcohols (Seo 2013). The high basal spacing might be attributed to incomplete removal of oxygen functionalities. Also, a precise examination of the XRD pattern of the rGO reduced by ScPrOH and ScBuOH revealed two peaks (at 23–25°), indicating that both rGOs retained at least two different interlayer spacings. The presence of multiple interlayer spacing may be associated with the carbon chain of ScPrOH and ScBuOH attached to the surface of rGO during reduction. The XRD pattern of graphene, GO and SCF-reduced GO and a comparison with the hydrazine-reduced GO are illustrated in Fig. 12.

Brunauer–Emmett–Teller (BET)

The surface area and pore volume of the graphene materials are determined via the nitrogen adsorption/desorption isotherm. GO sheets, tightly packed by hydrogen bonding network between the oxygenated functionalities, showed a relatively low BET surface area of 30 $m^2\ g^{-1}$ (Mungse 2014). As ScH_2O facilitates the elimination of oxygen functionalities and prevents the restacking of platelets in GO, mesopores and micropores are created during the processing, thus increasing the material surface area. Narrow micropores (~1.3–1.5 nm) and mesopores (> 5 nm) were formed on rGOs that were produced via ScH_2O reduction at 150–500 °C with surface area recorded over a range of 39.4–474 $m^2\ g^{-1}$ (Mungse 2014; Torres 2017). Researchers explored the synergistic effect of the simultaneous processing of FLGO reduction and gasification of glycerol under SCF conditions created by ScH_2O (Torres 2017). Although a remarkable increase in the surface area was recorded,

Table 2 Surface area and pore size of rGO reduced by various SCFs

Supercritical fluid	Surface area ($m^2\ g^{-1}$)	Mesopore size (nm)	Micropore size (nm)	Ref
ScH_2O	39.4–474	Not stated	Not stated	Mungse 2014)
ScH_2O	84–215	5–60	~1.3–1.5	Torres 2017)
$ScCO_2$	541	28	1–5	Zhou 2015)
ScMeOH	114.2	Not stated	Not stated	Nursanto 2011)
ScMeOH	54	Not stated	Not stated	Seo 2013)
ScEtOH	203	Not stated	Not stated	Seo 2013)
ScPrOH	35	Not stated	Not stated	Seo 2013)
Sc2IPA	126	Not stated	Not stated	Seo 2013)
ScBuOH	25	Not stated	Not stated	Seo 2013)

higher restacking and folding of the graphene layers with a consequent loss of porosity were also observed. The average surface area of rFLGO was 84–255 m^2 g^{-1} with a microspore size of 1.5 nm and wider mesopores at 5–60 nm. Conversely, the surface areas of rGOs reduced by various supercritical alcohols were in the range of 25–203 m^2 g^{-1} (Seo 2013; Nursanto 2011). The surface areas and pore size of rGO produced via various treatment methods are summarised in Table 2.

High-resolution transmission electron microscopy (HRTEM)

HRTEM examines the microstructural images of the graphene materials. The obtained results showed the porous nature of GO, which suggest the occurrence of carbon atom consumption and probable decomposition of carboxyl groups (O=C–O) to release CO_2 during reduction. The release of these functional groups is supported by the decrease in area % in the XPS spectra as illustrated in Fig. 14a and b (Seo 2013). The successful restoration of the graphitic structure in supercritical alcohol-treated rGO samples was observed in the hexagonal symmetrical crystalline structure under transmission electron microscopy (Seo 2013; Nursanto 2011). The images also revealed rGO sheets produced from supercritical alcohol reduction aggregated to form thicker graphene flakes and tend to corrugate at the edge of the sheet, as shown in Fig. 13. The scrolling and bending effects result in the formation of nanovoid, subsequently leading to increasing the surface area of rGO.

Reduction with SCF enhances the adhesion and dispersion of precursors to prevent the uncontrolled growth of particles on graphene. Ag (grain size of 2–6 nm) (Meng et al. 2016) and Co_3O_4 (3.2–8.8 nm) (Zhao 2012) NPs were found to anchor on the graphene sheets evenly. The uniform graphene–PVA composites at 30–50 µm (Sasikala 2018) were also produced from SCF-aided reduction.

X-ray photoelectron spectroscopy (XPS)

X-ray photoelectron spectroscopy is used to quantify the atomic composition of graphene materials. High-resolution C1*s* XPS spectra revealed the double-peak structure of GO is in the region of higher binding energy (Fig. 14a). The shift of C1*s* peak maxima towards a lower-binding energy region indicated the deoxygenation of GO and revealed the regeneration of sp^2 carbon under ScH_2O treatment. In addition, the relative percent intensities of carbon bonded to oxygen-containing functionalities decrease substantially with the increasing treatment temperature as illustrated in Figs. 14c and d due to the removal of functional groups during thermal processes. The broad tail associated with π–π^* at 290.2–290.9 eV indicates the regeneration of sp^2 carbon and the restoration of delocalised π conjugation in ScH_2O-treated GO (Mungse 2014; Torres 2017).

RGOs produced from both ScH_2O and ScEtOH treatment methods exhibit similar XPS patterns where the peak area of sp^2 graphitic carbon is significantly reduced due to the regeneration of sp^2 carbon, and the generation of peaks associated with oxygen functionalities is observed. XPS scans confirmed that rGO produced from supercritical alcohol reduction contains mainly or only carbon and oxygen species and no impurities were detected as illustrated in Fig. 14b (Seo 2013; Nursanto 2011). The C/O ratio of the produced rGO is in the range of 2.2–14.4 (Seo 2013; Nursanto 2011) with the carbon atomic % of GO increased from 66.41 to 92.24% after treating with ScMeOH (Nursanto 2011), which are relatively higher when compared to the use of conventional solvents such as hydrazine (Lei 2011; Shen 2012; Fernández-Merino 2010). The peak area of the sp^2 graphitic carbon was increased, and the π–π^* shake-up peak for rGOs indicates the restoration of aromatic structures after reduction. Similarly, the formation of C–C bonds is reflected as carbon peaks at 285.5 eV. Notably, the C/O ratio of atom-doped graphene composite generally increased from 1.3–1.89 to 2.9–5.94 (Meng et al. 2016; Zhao 2014; Sasikala 2018; Zhou 2015) after treating with SCF.

Summary of SCF-facilitated graphene synthesis and challenges to resolve

The synthesis of graphene materials via SCF exfoliation and/or reduction methods following discussions

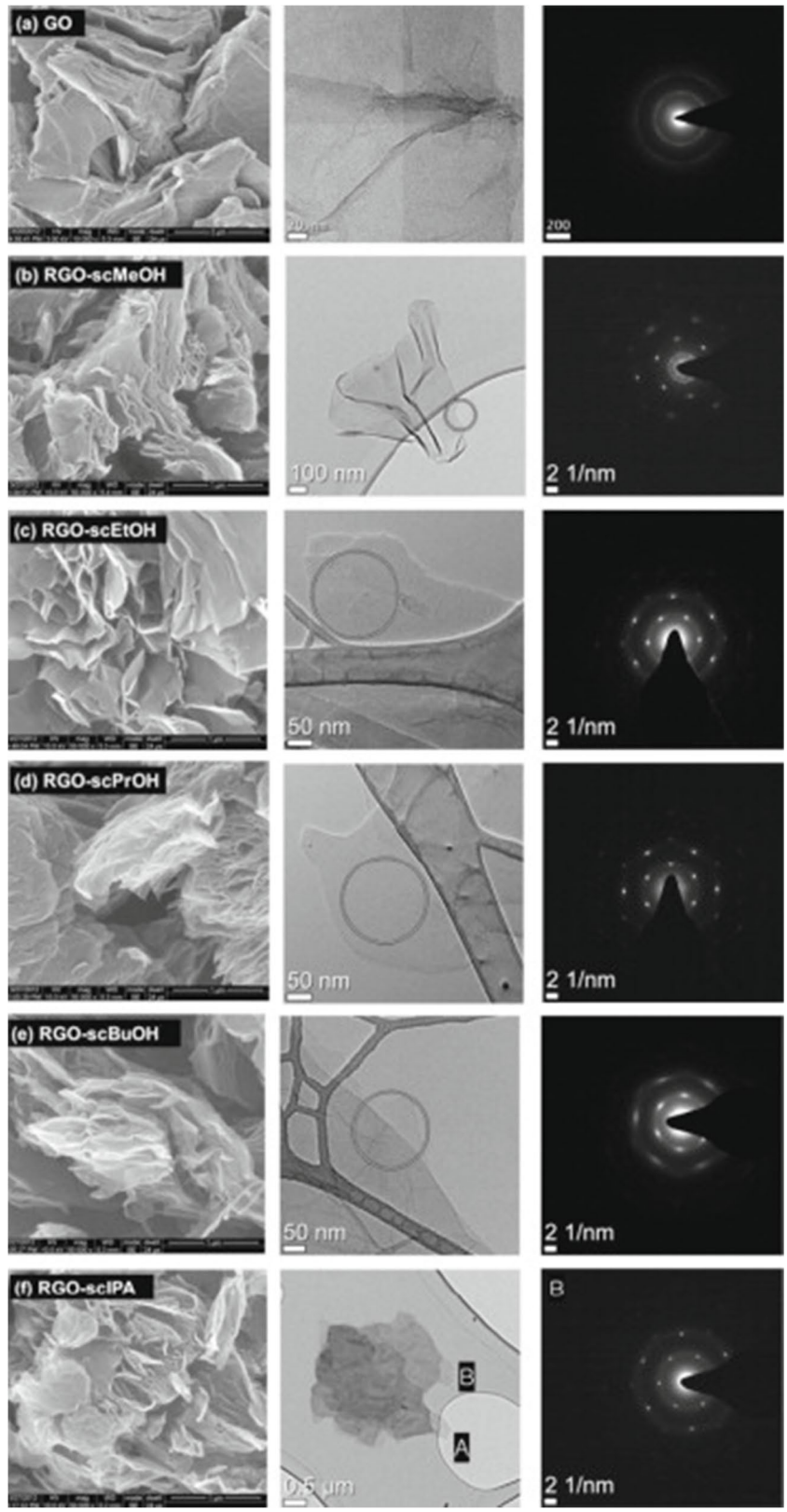

Fig. 13 (**a–f**) Electron microscopic images and selected area electron diffraction patterns of rGO using different supercritical alcohols (Seo 2013)

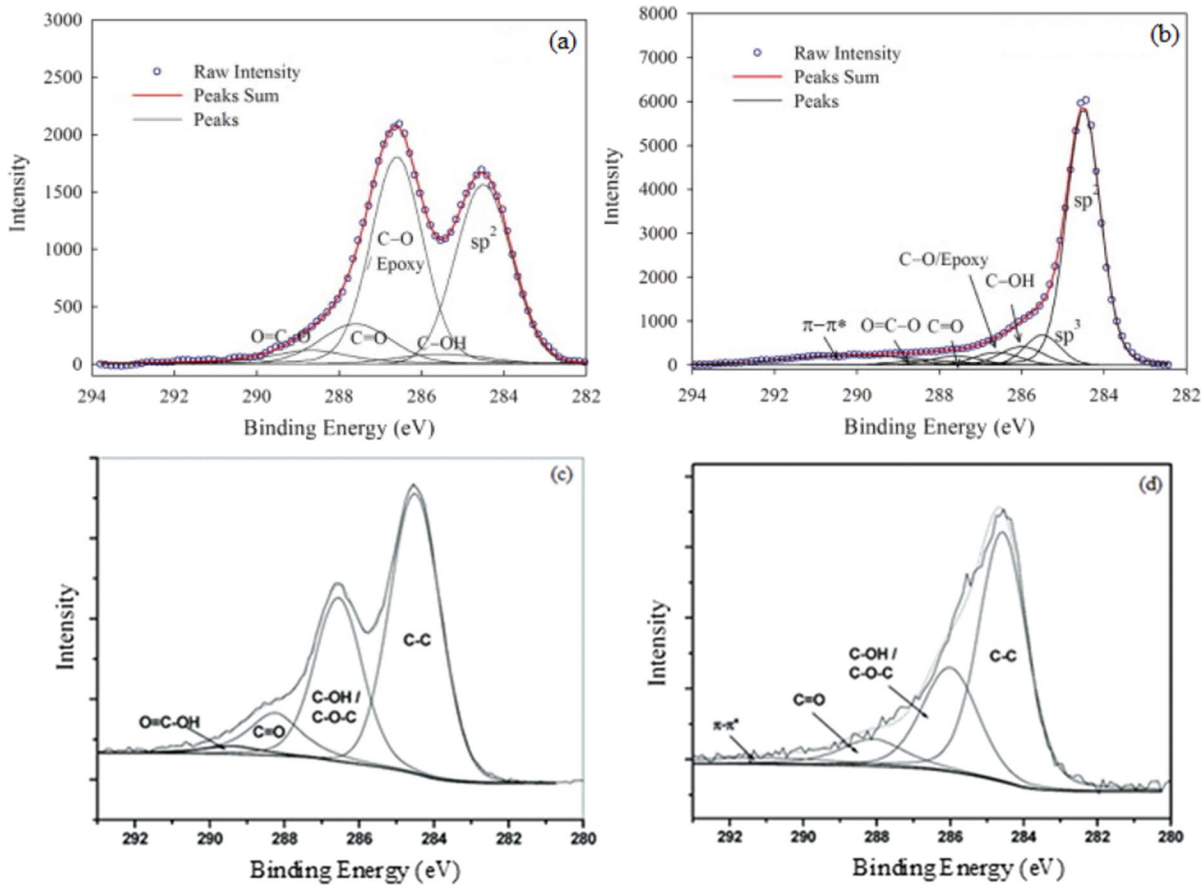

Fig. 14 XPS spectra of (**a**) GO, (**b**) rGO reduced by ScEtOH, (**c**) rGO reduced by ScH_2O at 99.85 °C and (**d**) rGO reduced by ScH_2O at 379.85 °C (Seo 2013; Mungse 2014)

in the previous sections are summarised in Tables 3 and 4.

Considering the impact of solvent usage on the environment, the use of SCFs with low boiling points, especially $ScCO_2$, is deemed to be a greener approach to other existing graphene production methods. Yet, exfoliation of graphite with $ScCO_2$ alone, by and large, produces graphene sheets of more than 10 layers, which is less than optimal. This is attributed to the non-polar nature of CO_2 and the rapid escape of CO_2 molecules from the intercalated layers (Sun et al. 2019). To resolve this issue and enhance the yield, it is common to recycle SCFs and repeat the exfoliation process, or even mix $ScCO_2$ with other solvents (Sim 2012). As it is, the use of co-solvent systems at supercritical state is becoming more common. The resultant mixture of solvents of different intrinsic chemical properties would have a significant influence on the process temperature and pressure to achieve the supercritical state, and would depend on the amount of contributing species present in the solvent (Sun et al. 2019). As for SCF reduction, the C/O ratios of graphene materials produced via SCF reduction are higher or comparable to those produced from other reduction techniques. This suggests that SCF might be a plausible reduction method to be scaled up for effective removal of oxygen functional groups from GO and restore the basal plane carbon structures of graphene. However, the mechanisms of reduction and the effect of various supercritical fluids on the properties of rGO have not been fully understood (Seo 2013; Mungse 2014).

SCF technology can be expensive, which is often perceived as a drawback (Sun et al. 2019). This is due to the extreme operating conditions requiring high temperature and pressure for the solvents to achieve supercritical state; hence, the reactors must

Table 3 Operating conditions and yield of SCF exfoliation of different precursors for graphene production

SCF	Precursor	Operating conditions	Reactor mode	Reaction time (min)	Yield	Ref
DMF, NMP, EtOH	Graphite crystals	300–400 °C, 38–40 MPa	Mechanical exfoliation	15–60	90–95% < 8 layers, 6–10% monolayers, 5–10% ≥ 10 layers	Rangappa, et al. 2010)
DMF	Expandable graphite powder	150–500 °C, 4.4 MPa	Not specified (n.s.)	15–45	7%	Liu et al. 2012)
Water	Graphite powder	400 °C, 29 MPa	Batch-type Inconel reactor, mechanical stirring at a frequency of 60 cycles per min	60	n.s	Morales Ibarra, et al. 2020)
EtOH-H_2O	Graphite powder	325–425 °C, 20–40 MPa	0–50% H_2O used as co-solvent	60	18.5%	Hadi 2016)
Ethanol	Graphite powder	260 °C, 7.8 MPa	Batch-type Inconel reactor, mechanical stirring at a frequency of 60 cycles per min	60	n.s	Morales Ibarra, et al. 2020)
Methanol	Acid-pretreated graphite flakes	300–400 °C, 38–40 MPa	n.s	30–60	n.s	(Rangappa et al. 2011)
NH_3	Graphite flakes	200 °C, 15 MPa	n.s	60–120	~3% (40% of it is < 5 layers)	Sasikala 2016)
CO_2	Graphite powder	45 °C, 10 MPa	Ultrasonic-assisted exfoliation, water bath with an ultrasonic probe at 45 kHz	60 min	n.s	Morales Ibarra, et al. 2020)
CO_2	Graphite powder and PVP dispersed in ethanol solution	40.05 °C, 16 MPa	Mechanically stirred exfoliation	180	38.6% (87.7% of 1.93 mg mL^{-1} of graphene is ≤ 3 layers)	Xu et al. 2015)
CO_2	Graphite powder with SDBS dispersed in ethanol solution	45 °C, 8–25 MPa	Shear mixer with a 25-mm 6 and 12-blade stator under a rotational speed of 1–3000 rpm	60–480	63.2% (where 27% of it is monolayer, 25% is bilayer and 14% is trilayer)	Song et al. 2016)

Table 4 Reduction performance of various SCFs for the production of graphene materials

SCF	Precursor	Operating conditions	Reaction time (min)	Final product	C/O ratio, *d* spacing	Ref
H_2O	GO	99.85–379.85 °C, 0.04–22.75 MPa	120–720	rGO	Not stated (n.s.), 0.35 nm	Mungse 2014)
H_2O	FLGO, glycerol	400–500 °C, 23 MPa	120	rFLGO	28.2, n.s	Torres 2017)
H_2O	GO, glycine	400 °C	60	N-doped rGO	n.s	Suresh Balaji et al. 2018)
H_2O	GO, dimethyl sulphoxide	400 °C	60	S-doped rGO	n.s	Balaji 2019)
CO_2	GO	< 300 °C, 10 MPa	120–300	rGO	n.s	Kong 2012)
CO_2	GO, silver ammonia	80 °C, 15 MPa	60	SAg/GN composite	4.5, n.s	Meng et al. 2016)
CO_2	GO, cobalt nitrate hexahydrate	150 °C, 9 MPa	1440	Co_3O_4/graphene oxide composites	2.9, n.s	Zhao 2014)
CO_2	Graphene sheets, platinum	n.s	n.s	Pt/graphene composite	n.s	Zhang et al. 2014)
CO_2	GP-PVA films	100–150 °C, 20–25 MPa	60–180	rGO-PEG and rGO-PVA fibres	5.94, n.s	Sasikala 2018)
CO_2	GO, borane–tetrahydrofuran (THF)	79.85 °C, 30.4 MPa	1440	B-doped rGO	5.9, 0.379–0.380 nm	Nursanto 2011)
MeOH	GO	400 °C, 36.5 MPa	120	rGO	10.4, 0.3693 nm	Seo 2013)
MeOH	GO	400 °C, 30 MPa	120	rGO	8.78–10.18, 0.356–0.359 nm	Nursanto 2011)
EtOH	GO, ascorbic acid	23 °C	1440	rGO	0.37, n.s	Zhang 2010)
EtOH	GO	400 °C, 25.2 MPa	120	rGO	14.4, 0.3654 nm	Seo 2013)
PrOH	GO	400 °C, 17.8 MPa	120	rGO	13.7, 0.3583–0.3739 nm	Seo 2013)
2IPA	GO	400 °C, 19.7 MPa	120	rGO	13.2, 0.3613 nm	Seo 2013)
BuOH	GO	400 °C, 12.9 MPa	120	rGO	12.5, 0.3599–0.3812 nm	Seo 2013)

be able to withstand such conditions. Another challenge is the storage of graphene and its composites prior to use. It is difficult to preserve and maintain the quality of the as-synthesised graphene, in particular graphene suspension. Graphene suspension has to be colloidally stable and remains dispersed in appropriate solvents ensuring good use for its intended application (Johnson et al. 2015). This is of utmost importance, where the storage and transfer of graphene products are as important as the manufacturing process.

Conclusion

Graphene with superior physicochemical properties has gained broad research interests with many applications exploring the advantages of incorporating graphene materials. Recognising the current limitations in graphene production due to the high cost involved with resulting low production yield that consequently restricted bulk production of graphene via existing technologies, attention has been shifted to the synthesis of high-quality graphene materials via SCF-aided exfoliation and reduction. A comprehensive review has been conducted featuring

recent works on graphene derived from SCFs along with the expositions of the mechanisms. Intercalation and exfoliation under SCF conditions imply rapid penetration of solvent molecules through the interlayers of graphite to overcome van der Waals forces and achieve delamination of graphitic materials. The incorporation of external forces such as sonication and stirring has proven to improve the process efficiency. Conversely, SCF reduction produces high-quality rGO by removing the oxygen functionalities and restoring the original graphene structure from GO. The conductivity and electrocatalytic properties were retained or even enhanced after SCF treatment, successfully meeting requirements for various applications in energy storage, capacitors and catalytic reactions. In summary, by selecting appropriate solvent and precursors or through materials co-processing, enhancement in graphene production could be achieved in terms of yield, morphology and characteristics. However, these achievements are conditioned by the prior success of addressing the full effect of SCF on exfoliation and the mechanisms of GO deoxygenation, towards realising commercialisation of high-quality graphene production.

Funding The authors gratefully express gratitude to all parties which have contributed towards the success of this project, both financially and technically, especially the S&T Innovation 2025 Major Special Programme (grant number 2018B10022) and the Ningbo Natural Science Foundation Programme (grant number 2018A610069) funded by the Ningbo Science and Technology Bureau, China, as well as the UNNC FoSE Faculty Inspiration Grant, China. The Zhejiang Provincial Department of Science and Technology is also acknowledged for this research under its Provincial Key Laboratory Programme (2020E10018).

Declarations

Conflict of interest The authors declare no competing interests.

References

Aissa B et al (2015) Recent progress in the growth and applications of graphene as a smart material: a review. Frontiers in Materials 2:58

Allen MJ, Tung VC, Kaner RB (2010) Honeycomb carbon: a review of graphene. Chem Rev 110(1):132–145

Amiri A et al (2018) A review on liquid-phase exfoliation for scalable production of pure graphene, wrinkled, crumpled and functionalized graphene and challenges. FlatChem 8:40–71

Andonovic B et al (2015) Enhanced model for determining the number of graphene layers and their distribution from X-ray diffraction data. Beilstein J Nanotechnol 6:2113–2122

Bagri A et al (2010) Structural evolution during the reduction of chemically derived graphene oxide. Nat Chem 2(7):581–587

Bahrami M, Ranjbarian S (2007) Production of micro- and nano-composite particles by supercritical carbon dioxide. J Supercritical Fluids 40(2):263–283

Balaji SS et al (2019) Supercritical fluid assisted synthesis of S-doped graphene and its symmetric supercapacitor performance evaluation using different electrolytes. Synthetic Metals 255:116111

Balandin AA et al (2008) Superior thermal conductivity of single-layer graphene. Nano Lett 8(3):902–907

Bastwros M et al (2014) Effect of ball milling on graphene reinforced Al6061 composite fabricated by semi-solid sintering. Compos B Eng 60:111–118

Beckman EJ (2004) Supercritical and near-critical CO_2 in green chemical synthesis and processing. The Journal of Supercritical Fluids 28(2):121–191

Berciaud S et al (2009) Probing the intrinsic properties of exfoliated graphene: Raman spectroscopy of free-standing monolayers. Nano Lett 9(1):346–352

Berger C et al (2004) Ultrathin epitaxial graphite: 2D electron gas properties and a route toward graphene-based nanoelectronics. J Phys Chem B 108(52):19912–19916

Bolotin KI et al (2008) Ultrahigh electron mobility in suspended graphene. Solid State Commun 146(9–10):351–355

Cano-Márquez AG et al (2009) Ex-MWNTs: graphene sheets and ribbons produced by lithium intercalation and exfoliation of carbon nanotubes. Nano Lett 9(4):1527–1533

Casiraghi C et al (2009) Raman spectroscopy of graphene edges. Nano Lett 9(4):1433–1441

Chen C-Y et al (2011) Uniform dispersion of Pd nanoparticles on carbon nanostructures using a supercritical fluid deposition technique and their catalytic performance towards hydrogen spillover. J Mater Chem 21(47):19063–19068

Chua CK, Pumera M (2014) Chemical reduction of graphene oxide: a synthetic chemistry viewpoint. Chem Soc Rev 43(1):291–312

Compton OC, Nguyen ST (2010) Graphene oxide, highly reduced graphene oxide, and graphene: versatile building blocks for carbon-based materials. Small 6(6):711–723

Cruz-Silva E et al (2009) Electronic transport and mechanical properties of phosphorus-and phosphorus–nitrogen-doped carbon nanotubes. ACS Nano 3(7):1913–1921

Cui X et al (2011) Liquid-phase exfoliation, functionalization and applications of graphene. Nanoscale 3(5):2118–2126

Dayou S et al (2017) High-rate synthesis of graphene by a lower cost chemical vapor deposition route. J Nanopart Res 19(10):336

Dreyer DR, Todd AD, Bielawski CW (2014) Harnessing the chemistry of graphene oxide. Chem Soc Rev 43(15):5288–5301

Eckert CA, Knutson BL, Debenedetti PG (1996) Supercritical fluids as solvents for chemical and materials processing. Nature 383(6598):313–318

Fan X et al (2016) Functionalized graphene nanoplatelets from ball milling for energy applications. Curr Opin Chem Eng 11:52–58

Fang Z et al (2020) Conversion of biological solid waste to graphene-containing biochar for water remediation: A critical review. Chem Eng J 390:124611

Fernández-Merino MJ et al (2010) Vitamin C is an ideal substitute for hydrazine in the reduction of graphene oxide suspensions. The Journal of Physical Chemistry C 114(14):6426–6432

Ferrari AC (2007) Raman spectroscopy of graphene and graphite: disorder, electron–phonon coupling, doping and nonadiabatic effects. Solid State Commun 143(1):47–57

Gai Y et al (2018) Ultrasound coupled with supercritical carbon dioxide for exfoliation of graphene: simulation and experiment. Ultrason Sonochem 41:181–188

Gao W et al (2009) New insights into the structure and reduction of graphite oxide. Nat Chem 1(5):403–408

Gao H et al (2017) Large-scale graphene production by ultrasound-assisted exfoliation of natural graphite in supercritical CO_2/H_2O medium. Chem Eng J 308:872–879

Gao H, Hu G (2016) Graphene production via supercritical fluids. RSC Adv 6(12):10132–10143

Geim AK, Novoselov KS (2010) The rise of graphene. Nanoscience and technology: a collection of reviews from nature journals. World Scientific, pp 11–19

Green AA, Hersam MC (2009) Solution phase production of graphene with controlled thickness via density differentiation. Nano Lett 9(12):4031–4036

Hadi A et al (2016) Optimization of graphene production by exfoliation of graphite in supercritical ethanol: a response surface methodology approach. The Journal of Supercritical Fluids 107:92–105

Hernandez Y et al (2008) High-yield production of graphene by liquid-phase exfoliation of graphite. Nat Nanotechnol 3(9):563–568

Hernandez Y et al (2010) Measurement of multicomponent solubility parameters for graphene facilitates solvent discovery. Langmuir 26(5):3208–3213

Hu W-C, Hou S-S, Lin T-H (2017) Transition of carbon nanostructures in heptane diffusion flames. J Nanopart Res 19(2):82

Jeon I-Y et al (2013) Facile, scalable synthesis of edge-halogenated graphene nanoplatelets as efficient metal-free eletrocatalysts for oxygen reduction reaction. Sci Rep 3:1810

Jeon I-Y et al (2017) Heavily aluminated graphene nanoplatelets as an efficient flame-retardant. Carbon 116:77–83

Jiao L et al (2009) Narrow graphene nanoribbons from carbon nanotubes. Nature 458(7240):877–880

Johnson DW, Dobson BP, Coleman KS (2015) A manufacturing perspective on graphene dispersions. Curr Opin Colloid Interface Sci 20(5):367–382

Jorio A, Martins Ferreira EH, Cançado, LG, Achete CA, Capaz RB (2011) Physics and applications of graphene – experiments. InTech Publishing

Karamat S et al (2015) Synthesis of few layer single crystal graphene grains on platinum by chemical vapour deposition. Progress in Natural Science: Materials International 25(4):291–299

Kharisov, BI and Kharissova OV (2009) Carbon allotropes: metal-complex chemistry, properties and applications. Springer International Publishing

Kong CY et al (2012) Supercritical fluid conversion of graphene oxides. The Journal of Supercritical Fluids 61:206–211

Kosynkin DV et al (2009) Longitudinal unzipping of carbon nanotubes to form graphene nanoribbons. Nature 458(7240):872–876

Kudin KN et al (2008) Raman spectra of graphite oxide and functionalized graphene sheets. Nano Lett 8(1):36–41

Kuijpers MWA et al (2002) Cavitation-induced reactions in high-pressure carbon dioxide. Science 298(5600):1969

Lee XJ et al (2012) Evaluation of carbon-based nanosorbents synthesised by ethylene decomposition on stainless steel substrates as potential sequestrating materials for nickel ions in aqueous solution. J Environ Sci 24(9):1559–1568

Lee G-H et al (2013) High-strength chemical-vapor–deposited graphene and grain boundaries. Science 340(6136):1073–1076

Lee XJ et al (2019) Review on graphene and its derivatives: synthesis methods and potential industrial implementation. J Taiwan Inst Chem Eng 98:163–180

Lee H, Park JY (2019) Height determination of single-layer graphene on mica at controlled humidity using atomic force microscopy. Review of Scientific Instruments 90(10):103702

Lei Y et al (2011) Hydrolysable tannin as environmentally friendly reducer and stabilizer for graphene oxide. Green Chem 13(7):1655–1658

Lerf A et al (1998) Structure of graphite oxide revisited. J Phys Chem B 102(23):4477–4482

Lester E et al (2018) A proposed biomass char classification system. Fuel 232:845–854

Li X et al (2009) Large-area synthesis of high-quality and uniform graphene films on copper foils. Science 324(5932):1312–1314

Li Z et al (2011a) Flame synthesis of few-layered graphene/graphite films. Chem Commun 47(12):3520–3522

Li Z et al (2011b) Ethanol flame synthesis of highly transparent carbon thin films. Carbon 49(1):237–241

Li L et al (2013) Solvent-exfoliated and functionalized graphene with assistance of supercritical carbon dioxide. ACS Sustainable Chemistry & Engineering 1(1):144–151

Liu L et al (2012) High-yield chemical vapor deposition growth of high-quality large-area AB-stacked bilayer graphene. ACS Nano 6(9):8241–8249

Liu L et al (2019a) Synergistic effect of supercritical CO_2 and organic solvent on exfoliation of graphene: experiment and atomistic simulation studies. Phys Chem Chem Phys 21(39):22149–22157

Liu Z et al (2019) Lateral size of graphene characterized by atomic force microscope. IOP Conf Ser Earth Environ Sci 252:022022

Liu Z, Han B (2009) Synthesis of carbon-nanotube composites using supercritical fluids and their potential applications. Adv Mater 21(7):825–829

Liu C, Hu G, Gao H (2012) Preparation of few-layer and single-layer graphene by exfoliation of expandable graphite in supercritical N. N-Dimethylformamide the Journal of Supercritical Fluids 63:99–104
Lozowski D (2010) Supercritical CO_2: a green solvent. Chem Eng 117(2):15
Manukyan KV et al (2013) Combustion synthesis of graphene materials. Carbon 62:302–311
Mao S, Pu H, Chen J (2012) Graphene oxide and its reduction: modeling and experimental progress. RSC Adv 2(7):2643–2662
Memon NK et al (2013) Role of substrate, temperature, and hydrogen on the flame synthesis of graphene films. Proc Combust Inst 34(2):2163–2170
Meng Y, Su F, Chen Y (2016) Supercritical fluid synthesis and tribological applications of silver nanoparticle-decorated graphene in engine oil nanofluid. Sci Rep 6:31246. https://doi.org/10.1038/srep31246
Min BH et al (2014) Bulk scale growth of CVD graphene on Ni nanowire foams for a highly dense and elastic 3D conducting electrode. Carbon 80:446–452
Mishra N et al (2016) Graphene growth on silicon carbide: a review. physica status solidi (a) 213(9):2277–2289
Mondal S, Ghosh S, Raj CR (2018) Unzipping of single-walled carbon nanotube for the development of electrocatalytically active hybrid catalyst of graphitic carbon and Pd nanoparticles. ACS Omega 3(1):622–630
Morales Ibarra R et al (2020) Graphene exfoliation with supercritical fluids. Carbon Letter 31:99–105
Mungse HP et al (2014) Hydrothermal deoxygenation of graphene oxide in sub- and supercritical water. RSC Adv 4(43):22589–22595
Nakagawa T et al (2003) Reactions of supercritical alcohols with unsaturated hydrocarbons. The Journal of Supercritical Fluids 27(3):255–261
National Center for Biotechnology Information (2004) PubChem compound summary for CID 6228, N,N-dimethylformamide. National Center for BiotechnologyInformation, Bethesda
National Center for Biotechnology Information (2004) PubChem annotation record for 1-methyl-2-pyrrolidinone. National Center for Biotechnology Information, Bethesda
Nursanto EB et al (2011) Facile synthesis of reduced graphene oxide in supercritical alcohols and its lithium storage capacity. Green Chem 13(10):2714–2718
Obraztsov A et al (2007) Chemical vapor deposition of thin graphite films of nanometer thickness. Carbon 45(10):2017–2021
Ossler F et al (2010) Sheet-like carbon particles with graphene structures obtained from a Bunsen flame. Carbon 48(14):4203–4206
Padmajan Sasikala S, Poulin P, Aymonier C (2016) Prospects of supercritical fluids in realizing graphene-based functional materials. Advanced Materials 28(14):2663–2691
Pan F et al (2013) Advanced oxygen reduction electrocatalyst based on nitrogen-doped graphene derived from edible sugar and urea. ACS Appl Mater Interfaces 5(21):11108–11114
Pang CH, Lester E, Wu T (2018) Influence of lignocellulose and plant cell walls on biomass char morphology and combustion reactivity. Biomass Bioenerg 119:480–491
Parvez AM et al (2016) Effect of the addition of different waste carbonaceous materials on coal gasification in CO_2 atmosphere. Fuel Process Technol 149:231–238
Pruna A, Pullini D, Busquets D (2013) Influence of synthesis conditions on properties of green-reduced graphene oxide. J Nanopart Res 15(5):1605
Qu L et al (2010) Nitrogen-doped graphene as efficient metal-free electrocatalyst for oxygen reduction in fuel cells. ACS Nano 4(3):1321–1326
Rangappa D et al (2010) Rapid and direct conversion of graphite crystals into high-yielding, good-quality graphene by supercritical fluid exfoliation. Chemistry – A European Journal 16(22):6488–6494
Rangappa D, Jang JH, Honma I (2011) Graphene - Synthesis, Characterization, Properties and Applications. BoD – Books on Demand
Ray AK et al (2012) Preparation and characterization of graphene and Ni-decorated graphene using flower petals as the precursor material. Carbon 50(11):4123–4129
Ross DS, Blessing JE (1979) Alcohols as H-donor media in coal conversion. 2 Base-promoted H-donation to coal by methyl alcohol. Fuel 58(6):438–442
Ruan G et al (2011) Growth of graphene from food, insects, and waste. ACS Nano 5(9):7601–7607
Salem ML et al (2020) Superparamagnetic graphene oxide/magnetite nanocomposite delivery system for doxorubicin-induced distinguished tumor cell cycle arrest and apoptosis. J Nanopart Res 22(8):219
Sasikala SP et al (2016) Simultaneous graphite exfoliation and N doping in supercritical ammonia. ACS Appl Mater Interfaces 8(45):30964–30971
Sasikala SP et al (2018) An effective in situ reduction strategy assisted by supercritical fluids for the preparation of graphene - polymer composites. Carbon 139:572–580
Seo M et al (2013) Supercritical alcohols as solvents and reducing agents for the synthesis of reduced graphene oxide. Carbon 64:207–218
Serhatkulu GK, Dilek C, Gulari E (2006) Supercritical CO_2 intercalation of layered silicates. The Journal of Supercritical Fluids 39(2):264–270
Shearer CJ et al (2016) Accurate thickness measurement of graphene. Nanotechnology 27(12):125704
Shen J et al (2012) One-step solid state preparation of reduced graphene oxide. Carbon 50(6):2134–2140
Shin HJ et al (2009) Efficient reduction of graphite oxide by sodium borohydride and its effect on electrical conductance. Adv Func Mater 19(12):1987–1992
Sim HS et al (2012) Preparation of graphene nanosheets through repeated supercritical carbon dioxide process. Mater Lett 89:343–346
Singh V et al (2011) Graphene based materials: past, present and future. Prog Mater Sci 56(8):1178–1271
Somani PR, Somani SP, Umeno M (2006) Planer nano-graphenes from camphor by CVD. Chem Phys Lett 430(1–3):56–59
Song N et al (2016) Green production of pristine graphene using fluid dynamic force in supercritical CO_2. Chem Eng J 298:198–205
Stankovich S et al (2006) Stable aqueous dispersions of graphitic nanoplatelets via the reduction of exfoliated

graphite oxide in the presence of poly(sodium 4-styrenesulfonate). J Mater Chem 16(2):155–158
Sun Z et al (2019) Supercritical fluid-facilitated exfoliation and processing of 2D materials. Advanced Science 6(18):1901084
Suresh Balaji S, Karnan M, Sathish M (2018) Supercritical fluid processing of N-doped graphene and its application in high energy symmetric supercapacitor. International Journal of Hydrogen Energy 43(8):4044–4057
Szabó T et al (2006) Evolution of surface functional groups in a series of progressively oxidized graphite oxides. Chem Mater 18(11):2740–2749
Tao H et al (2017) Scalable exfoliation and dispersion of two-dimensional materials – an update. Phys Chem Chem Phys 19(2):921–960
Thess A et al (1996) Crystalline ropes of metallic carbon nanotubes. Science 273(5274):483–487
Tiwary CS et al (2015) Chemical-free graphene by unzipping carbon nanotubes using cryo-milling. Carbon 89:217–224
Tomai T, Kawaguchi Y, Honma I (2012) Nanographene production from platelet carbon nanofiber by supercritical fluid exfoliation. Applied Physics Letters 100(23):233110
Torres D et al (2017) Enhanced reduction of few-layer graphene oxide via supercritical water gasification of glycerol. Nanomaterials (basel, Switzerland) 7(12):447
Tung VC et al (2009) High-throughput solution processing of large-scale graphene. Nat Nanotechnol 4(1):25
Tuz Johra, F, Lee J, and Jung WG (2014) Facile and safe graphene preparation on solution based platform. J Ind Eng Chem 20:2883–2887
Wang X et al (2009) Large-scale synthesis of few-layered graphene using CVD. Chem Vap Deposition 15(1–3):53–56
Wang W et al (2018) Highly efficient production of graphene by an ultrasound coupled with a shear mixer in supercritical CO_2. Ind Eng Chem Res 57(49):16701–16708
Wang D, Montané D, Chornet E (1996) Catalytic steam reforming of biomass-derived oxygenates: acetic acid and hydroxyacetaldehyde. Appl Catal A 143(2):245–270
World Helth Organization (2001) N-Methyl-2-pyrrolidone. In: Concise International Chemical Assessment Document. The World Health Organization, Lund
Wu N et al (2012) Synthesis of network reduced graphene oxide in polystyrene matrix by a two-step reduction method for superior conductivity of the composite. J Mater Chem 22(33):17254–17261
Wu B, Yang X (2011) A molecular simulation of interactions between graphene nanosheets and supercritical CO_2. J Colloid Interface Sci 361(1):1–8
Xu G et al (2012) Preparation of graphene oxide/polyaniline nanocomposite with assistance of supercritical carbon dioxide for supercapacitor electrodes. Ind Eng Chem Res 51(44):14390–14398
Xu S et al (2015) Reverse-micelle-induced exfoliation of graphite into graphene nanosheets with assistance of supercritical CO_2. Chem Mater 27(9):3262–3272
Xu Q-Q et al (2018) Exfoliation of graphite in CO_2 expanded organic solvents combined with low speed shear mixing. Carbon 135:180–186
Yan J et al (2016) Influence of minerals on the thermal processing of bamboo with a suite of carbonaceous materials. Fuel 180:256–262
Yannopoulos SN et al (2012) CO_2 laser-induced growth of epitaxial graphene on 6H-SiC(0001). Adv Func Mater 22(1):113–120
Yi M et al (2012) A mixed-solvent strategy for facile and green preparation of graphene by liquid-phase exfoliation of graphite. J Nanopart Res 14(8):1003
Yi M et al (2013) Controllable functionalization and wettability transition of graphene-based films by an atomic oxygen strategy. J Nanopart Res 15(8):1811
Yi M, Shen Z (2015) A review on mechanical exfoliation for the scalable production of graphene. Journal of Materials Chemistry A 3(22):11700–11715
Yu Q et al (2008) Graphene segregated on Ni surfaces and transferred to insulators. Applied Physics Letters 93(11):113103
Zhang J et al (2010) Reduction of graphene oxide via L-ascorbic acid. Chem Commun 46(7):1112–1114
Zhang X, Heinonen S, Levänen E (2014) Applications of supercritical carbon dioxide in materials processing and synthesis. RSC Adv 4(105):61137–61152
Zhao J et al (2012) Decoration of ultrafine platinum-ruthenium particles on functionalized graphene sheets in supercritical fluid and their electrocatalytic property. J Nanopart Res 14(9):935
Zhao J et al (2014) Fabrication of Co_3O_4/graphene oxide composites using supercritical fluid and their catalytic application for the decomposition of ammonium perchlorate. CrystEngComm 16(10):2001–2008
Zhao H et al (2015) Screening of metal oxidesfor Hg^0capture. Energy Procedia 75:2421–2426
Zhao H et al (2016) Hg^0-temperature-programmed surface reaction and its application on the investigation of metal oxides for Hg^0 capture. Fuel 181:1089–1094
Zhao H et al (2020) MoO_3-adjusted δ-MnO_2 nanosheet for catalytic oxidation of Hg^0 to Hg^{2+}. Appl Catal B: Environ 263:117829
Zheng X et al (2012) High-throughput, direct exfoliation of graphite to graphene via a cooperation of supercritical CO_2 and pyrene-polymers. RSC Adv 2(28):10632–10638
Zhou Y et al (2015) One-pot synthesis of B-doped three-dimensional reduced graphene oxide via supercritical fluid for oxygen reduction reaction. Green Chem 17(6):3552–3560
Zhu Y et al (2010) Graphene and graphene oxide: synthesis, properties, and applications. Adv Mater 22(35):3906–3924